Supplementary information for:

Functional Off-stoichiometry in $Cu(In,Ga)Se_2$. Part II: Electronic Properties in a Wide Range of Compositions

Kostiantyn V. Sopiha[1,*], Jan Keller[1], Clas Persson[2], Jonathan J. S. Scragg[1], Charlotte Platzer-Björkman[1,3], and Marika Edoff[1]

1 – Division of Solar Cell Technology, Department of Materials Science and Engineering, Uppsala University, Box 534, SE-75237 Uppsala, Sweden
2 – Department of Materials Science and Engineering, KTH Royal Institute of Technology, SE-10044 Stockholm, Sweden
3 – Wallenberg Initiative Materials Science for Sustainability, Department of Materials Science and Engineering, Uppsala University, Box 534, SE-75237 Uppsala, Sweden

* **Corresponding author**: K. V. Sopiha (kostiantyn.sopiha@angstrom.uu.se)

Keywords: Copper deficiency, ordered vacancy compounds, topotactic transformation series, band gap widening, Fermi surfaces, transport anisotropy.

Table S1. Band gap energies (E_g) of different literature structures computed using the PBE+U functional after geometry optimization. All gaps are scissor-corrected by +0.93 and +1.20 eV for the Cu-In-Se and Cu-Ga-Se systems, respectively (same as in Fig. 2). The enthalpies above the hull (ΔH_{hull}) or formation enthalpies relative to the ground state (ΔH_f) are presented alongside the band gap; these values were computed using the PBE (without parentheses) and PBEsol (within parentheses) functionals in Part I of this study. The light green, pink, blue, and black spheres in the figures represent Se anions, group-III cations, Cu cations, and vacancies, respectively.

Literature source and identifier	Space group	ΔH_{hull} [meV/atom]		E_g [eV]		Structures (not optimized)
		$CuIn_5Se_8$	$CuGa_5Se_8$	$CuIn_5Se_8$	$CuGa_5Se_8$	
"Type-A" in Refs. #1,2 "mp-1212167" in Ref. #3 "$P\bar{4}2m$" in Ref. #4,5 Entry ID: 1731504 (also 6620 and 1731502) in Ref. #6	$P\bar{4}2m$	6.4 (7.9)	10.5 (10.2)	1.25	1.70	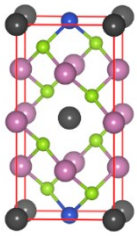
"Type-B" in Refs. #1,2	$P\bar{4}2m$	7.2 (8.4)	10.8 (9.7)	1.24	1.69	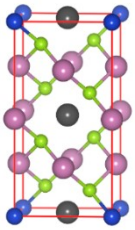
"Type-C" in Refs. #1,2	$I\bar{4}m2$	6.3 (6.9)	13.4 (11.5)	1.07	1.40	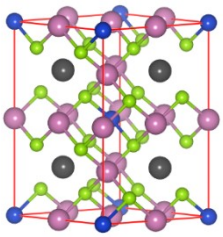
"Type-D" in Refs. #1,2 Zhang *et al.*[7,8] Ghorbani *et al.*[9] Kiss *et al.*[10,11] Xiao and Goddard[12] Pohl and Albe[13] Malitckaya *et al.*[14]	$C2$	2.2 (3.1)	4.1 (4.1)	1.23	1.69	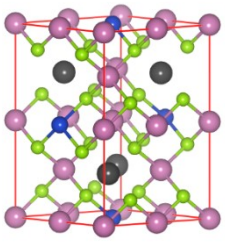
"Type-E" in Refs. #1,2 Sharan *et al.*[15] Maeda *et al.*[16] Jiang and Feng[17] Kumar *et al.*[18] Tu *et al.*[19]	$P\bar{4}$	10.5 (10.4)	12.7 (11.8)	1.24	1.79	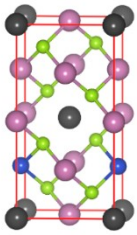

"Type-F" in Refs. #1,2 Jiang and Feng[17]	$P222$	12.2 (12.2)	15.8 (13.3)	1.23	1.78	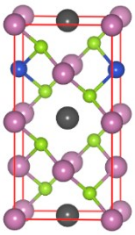
"New-1" in Ref. #1	$P\bar{4}n2$	3.3 (4.4)	8.3 (8.5)	1.14	1.49	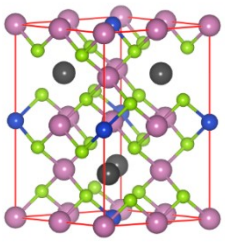
"New-2" in Ref. #1	$Amm2$	4.5 (5.7)	8.3 (7.6)	1.12	1.60	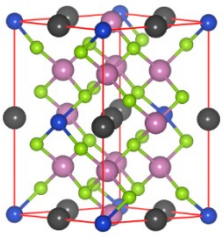
"$C222$" in Liu *et al.*[4]	$C222$	3.7 (4.0)	6.7 (4.8)	1.36	1.88	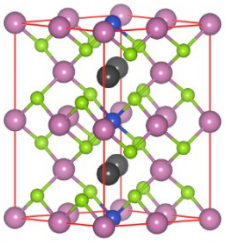
Part I of this study (ground state)	$Aea2$	0.0 (0.1)	0.0 (0.0)	1.31	1.98	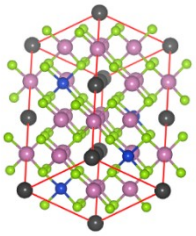
Part I of this study (slightly less stable)	$Iba2$	0.0 (0.0)	0.6 (0.4)	1.39	2.03	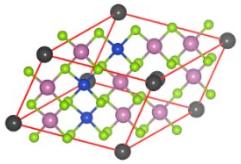

Literature source and identifier	Space group	ΔH_{hull} [meV/atom]		E_g [eV]		Structures (not optimized)
		$CuIn_3Se_5$	$CuGa_3Se_5$	$CuIn_3Se_5$	$CuGa_3Se_5$	
Refs. #3–5	$P1$	6.5 (7.6)	5.4 (5.6)	1.36	2.07	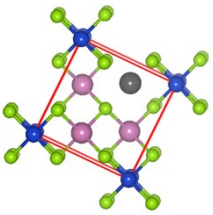
Part I of this study (ground state)	Cc	0.0 (0.0)	0.0 (0.0)	1.19	1.91	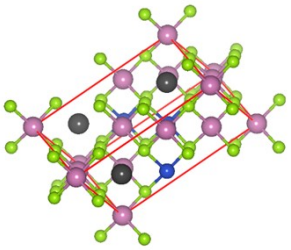
Lehmann *et al.*[20] for $CuIn_3Se_5$	$I\bar{4}2m$	--	--	--	--	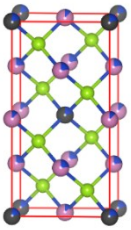
Lehmann *et al.*[20] for $CuGa_3Se_5$	$I\bar{4}2m$	--	--	--	--	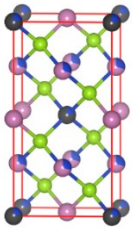
Literature source and identifier	Space group	ΔH_{hull} [meV/atom]		E_g [eV]		Structures (not optimized)
		$Cu_2In_4Se_7$	$Cu_2Ga_4Se_7$	$Cu_2In_4Se_7$	$Cu_2Ga_4Se_7$	
Yarema *et al.*[21] for $Cu_2In_4Se_7$	$P3_2$	29.2 (30.1)	31.1 (31.4)	1.23	1.80	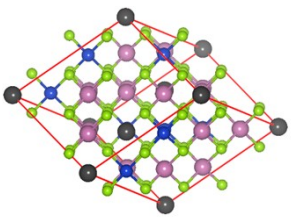

Part I of this study (ground state)	$C2$	0.0 (0.0)	0.0 (0.3)	1.20	1.89	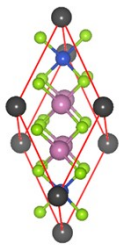
Literature source and identifier	Space group	ΔH_{hull} [meV/atom]		E_g [eV]		Structures (not optimized)
		$Cu_3In_5Se_9$	$Cu_3Ga_5Se_9$	$Cu_3In_5Se_9$	$Cu_3Ga_5Se_9$	
Yarema *et al.*[21] for $Cu_3In_5Se_9$	$P3_2$	16.6 (17.5)	18.8 (19.1)	1.05	1.63	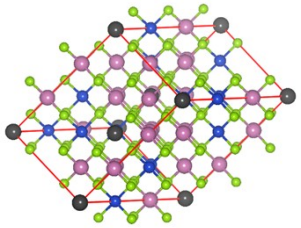
Moser *et al.*[22] for $Ag_3In_5Se_9$ (wurtzite lattice)	$P2_1$	11.5 (11.2)	13.9 (13.5)	1.15	1.73	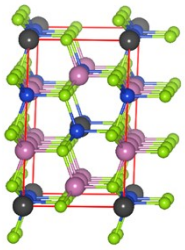
Part I of this study (ground state)	$C2$	0.0 (0.0)	0.0 (0.4)	1.15	1.83	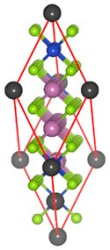
Literature source and identifier	Space group	ΔH_f [meV/atom]		E_g [eV]		Structures (not optimized)
		$CuInSe_2$	$CuGaSe_2$	$CuInSe_2$	$CuGaSe_2$	
Chalcopyrite	$I\bar{4}2d$	0.0 (0.0)	0.0 (0.0)	0.99	1.67	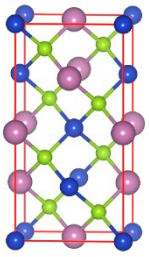

CuAu-type	$P\bar{4}m2$	2.2 (2.3)	9.7 (9.0)	Falsely metallic with PBE+U	1.32	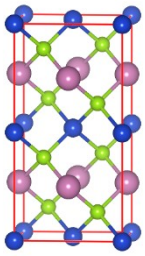

Table S2. Literature data of band gaps (E_g) measured for different compositions in the Cu-In-Se and Cu-Ga-Se systems. For incomplete and conflicting datasets, rational estimations are made, with room-temperature values and ODC-like structures taking precedence (although add-mixtures of hexagonal γ-CISe are likely to yield errors – the values for samples with γ-CISe signature are marked by asterisks). When not state by the source, the atomic fractions were inferred from the compound formulae and given in parentheses below. All band gaps from this table are collectively depicted in Fig. 2 as the "literature" scatterplot.

Suggested ODC (or phase)	[Cu] [at.%]	[In] [at.%]	[Se] [at.%]	E_g [eV]	Literature source
1:3:5	11.7	31.1	57.1	1.22	Marín *et al.*[23]
1:3:5	9.5	29.2	61.3	1.20	Rincón *et al.*[24]
1:3:5	(11.111)	(33.333)	(55.556)	1.154	Marín *et al.*[25]
1:3:5	10.69	33.85	55.46	1.26	Kim *et al.*[26]
1:3:5	11.7	32.6	55.7	1.23	Negami *et al.*[27]
2:4:7/1:3:5	16.6	31.1	52.3	1.15	León *et al.*[28,29]
1:1:2	(25)	(25)	(50)	1.05	Contreras *et al.*[30]
1:1:2	(25)	(25)	(50)	1.04	Alonso *et al.*[31]
1:1:2	(25)	(25)	(50)	0.99	Maeda *et al.*[16]
(α-phase)	21.951	26.829	51.22	0.99	
(β-phase)	13.636	31.818	54.545	1.13	
1:3:5	(11.111)	(33.333)	(55.556)	1.17	
(β-phase)	8.696	34.783	56.522	1.22*	
1:5:8	(7.143)	(35.714)	(57.143)	1.23*	
1:5:8	7.90	36.65	54.25	1.21*	Levcenko *et al.*[32]
				1.238*	
1:3:5	12.9	26.5	60.6	1.09	Friedrich *et al.*[33]
1:3:5	14.8	28.2	57.0	1.18	
2:4:7	16.0	33.6	50.4	1.22	Reddy and Raja[34]
1:3:5	(11.111)	(33.333)	(55.556)	1.31	Schmid *et al.*[35]
1:5:8	(7.143)	(35.714)	(57.143)	1.17*	Durán *et al.*[36]
1:5:8	7	36	57	1.31	Philip and Pradeep[37]
1:1:2	24	27	49	0.98	
1:3:5	11.2	35.6	53.2	1.23	Ariswan *et al.*[38]
1:3:5	11.9	37.9	50.2	1.23	
1:5:8	(7.143)	(35.714)	(57.143)	1.13*	Hernández *et al.*[39]
Suggested ODC	*[Cu] [at.%]*	*[Ga] [at.%]*	*[Se] [at.%]*	*Band gap [eV]*	*Literature source*
1:3:5	(11.111)	(33.333)	(55.556)	1.86	Marín *et al.*[40] Rincón *et al.*[24]
1:3:5	(11.111)	(33.333)	(55.556)	1.81	
1:3:5	(11.111)	(33.333)	(55.556)	1.818	
1:3:5	(11.111)	(33.333)	(55.556)	1.833	
1:3:5	(11.111)	(33.333)	(55.556)	1.754	Marín *et al.*[25]
1:3:5	11.4	32.1	56.5	1.85	Negami *et al.*[27]
1:3:5	13.1	34.55	52.35	1.88	León *et al.*[28,29]
1:3:5	12.7	35.08	52.22	1.88	
1:5:8	8.73	37.05	54.2	1.88	
1:1:2	(25)	(25)	(50)	1.67	Contreras *et al.*[30]
1:1:2	(25)	(25)	(50)	1.648	Alonso *et al.*[31]
1:1:2	(25)	(25)	(50)	1.68	Shay and Tell[41]

1:3:5	(11.111)	(33.333)	(55.556)	1.85	Ueda *et al.*[42]
1:3:5	11.7	32.2	56.1	1.71	Levcenko *et al.*[43]
1:5:8	(7.143)	(35.714)	(57.143)	1.852	Wasim *et al.*[44]
1:5:8	8.9	24.1	67.0	1.97	Friedrich *et al.*[33]
1:5:8	7.9	24.8	67.3	2.01	
1:5:8	7.6	22.1	70.3	1.76	
1:3:5	8.2	28.0	63.8	1.88	
1:3:5	6.8	23.8	69.4	1.97	
1:5:8	(7.143)	(35.714)	(57.143)	1.82	Durán *et al.*[36]

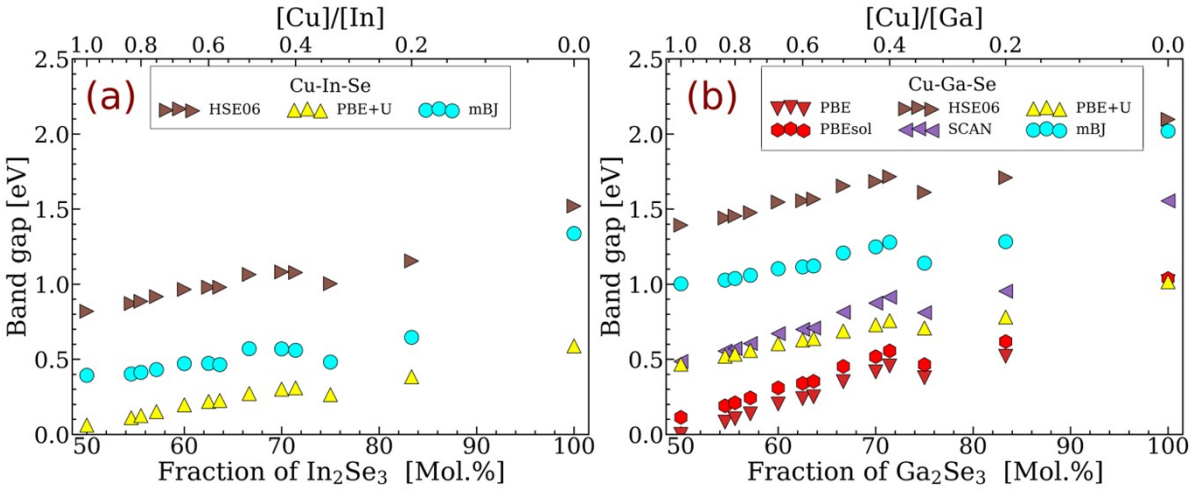

Figure S1. As-computed band gap energies of the (near-)stable zinc-blende-derived structures in the (a) Cu-In-Se and (b) Cu-Ga-Se systems computed using different functionals (no scissor correction applied). Besides the four functionals used for the analysis of electronic properties in the main text, the results obtained with the SCAN and PBEsol functionals are provided for comparison. All results except the mBJ-computed were obtained for the structures optimized with the corresponding functional. For the band gaps computed using mBJ, which is a potential-only functional, the PBEsol-optimized geometries were analyzed instead. The effect of structural relaxation on the band gap is illustrated in Fig. S2. The results from the PBE, PBEsol, and SCAN calculations are excluded for the Cu-In-Se system because some structures are erroneously metallic, due to the well-known band gap underestimation error.

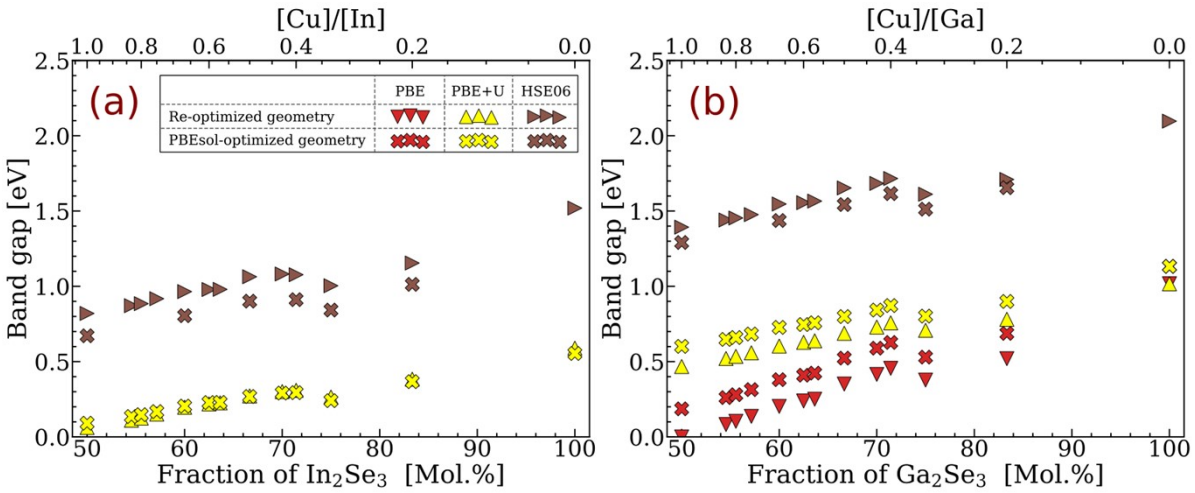

Figure S2. Comparison of the as-computed band gaps determined with different functionals in the (a) Cu-In-Se and (b) Cu-Ga-Se systems with and without structural optimization. The PBE results are excluded for the Cu-In-Se system because some structures are erroneously metallic, due to the well-known band gap underestimation error.

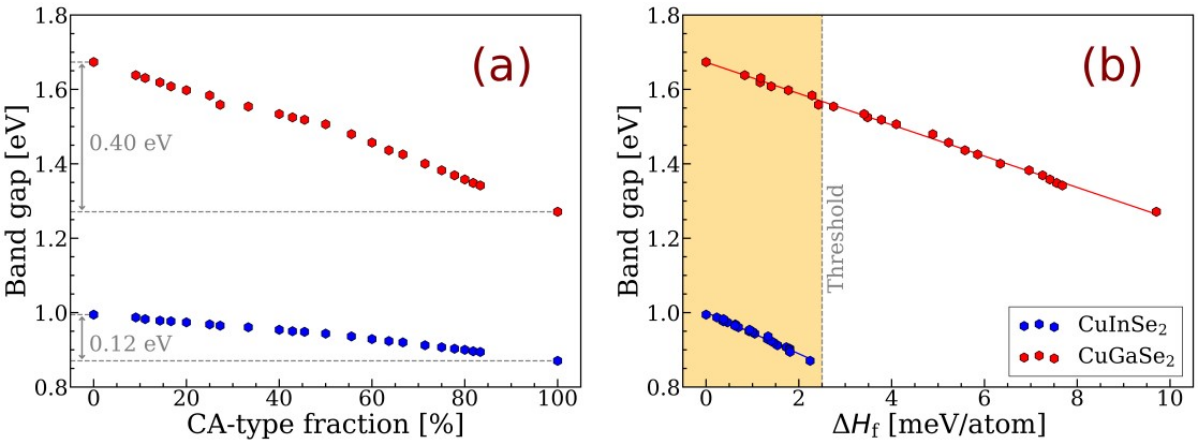

Figure S3. Computed band gap energies as functions of (a) CA-type fraction and (b) formation enthalpy relative to the ground state (ΔH_f) for various 1:1:2 polytypes. All band gaps here were calculated using the PBE+U functional (after geometry optimization) with a Hubbard U correction of 8 eV applied to the Cu 3d orbitals, which prevents the falsely metallic character observed in most $CuInSe_2$ polytypes when the default parameter is used. The scissor corrections were adjusted to +0.69 eV for $CuInSe_2$ and +0.96 eV for $CuGaSe_2$ polytypes. The formation enthalpies were computed using the PBE functional in Part I of this study.

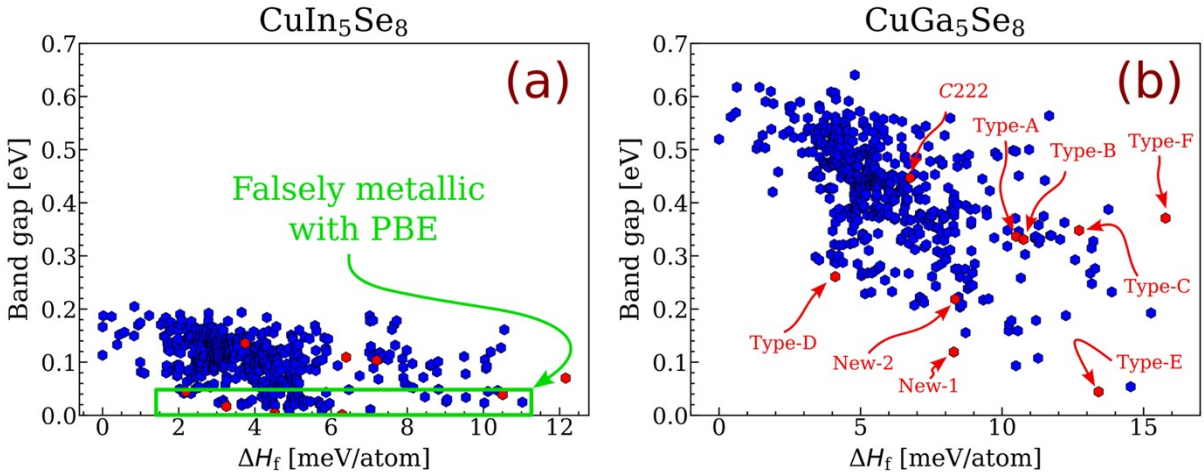

Figure S4. Band gap energies of various (a) $CuIn_5Se_8$ and (b) $CuGa_5Se_8$ polytypes as a function of their formation enthalpies relative to the ground state (ΔH_f). The data was computed using the PBE functional during the high-throughput screening described in Part I. The red and blue markers denote literature-reported structures and structures generated in the screening, respectively. Note that many $CuIn_5Se_8$ polytypes are incorrectly predicted to be metallic by the PBE functional.

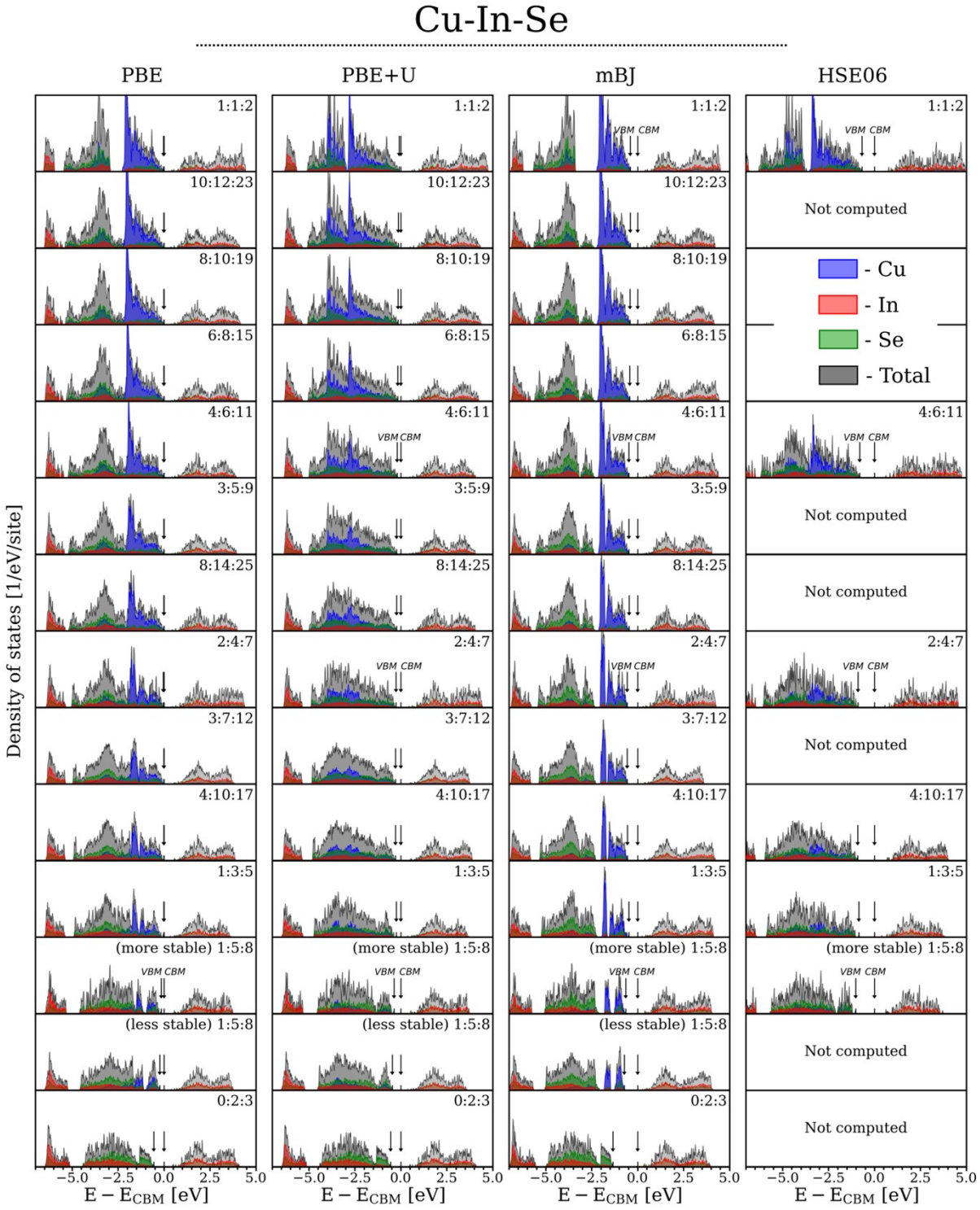

Figure S5. Densities of states for different (near-)stable Cu-In-Se phases computed with different functionals. All calculations were done for the PBEsol-optimized geometries. No adjustment of the band gaps was performed. In contrast to Fig. 3, all DOS presented here were computed using a relatively loose k-point grid density of 3000 (for PBE, PBE+U, and mBJ) or 1500 (for HSE06) points per reciprocal atom, and the cut-off energy specified in the Methods section.

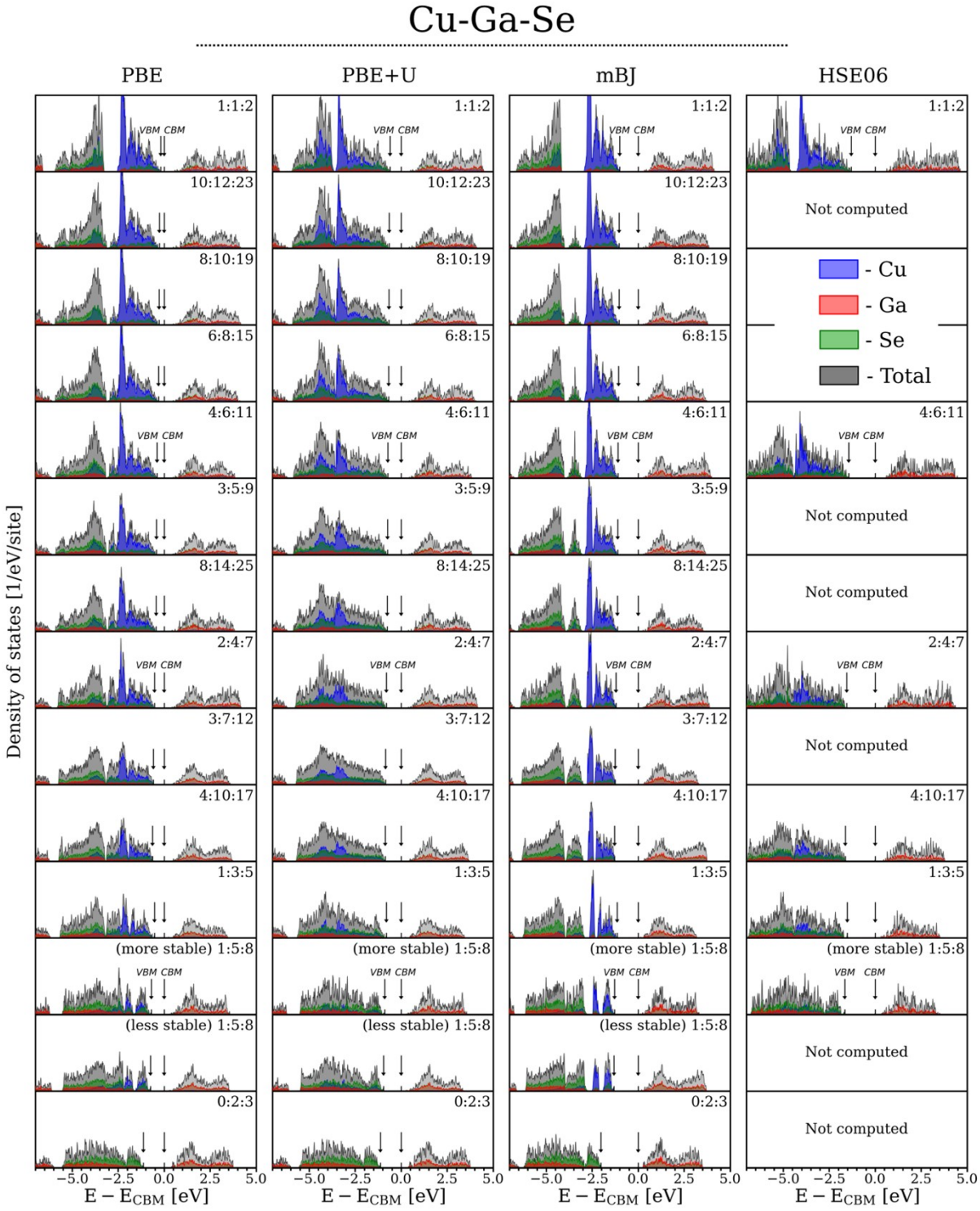

Figure S6. Densities of states for different (near-)stable Cu-Ga-Se phases computed with different functionals. All calculations were done for the PBEsol-optimized geometries. No adjustment of the band gaps was performed. In contrast to Fig. 3, all DOS presented here were computed using a relatively loose k-point grid density of 3000 (for PBE, PBE+U, and mBJ) or 1500 (for HSE06) points per reciprocal atom, and the cut-off energy specified in the Methods section.

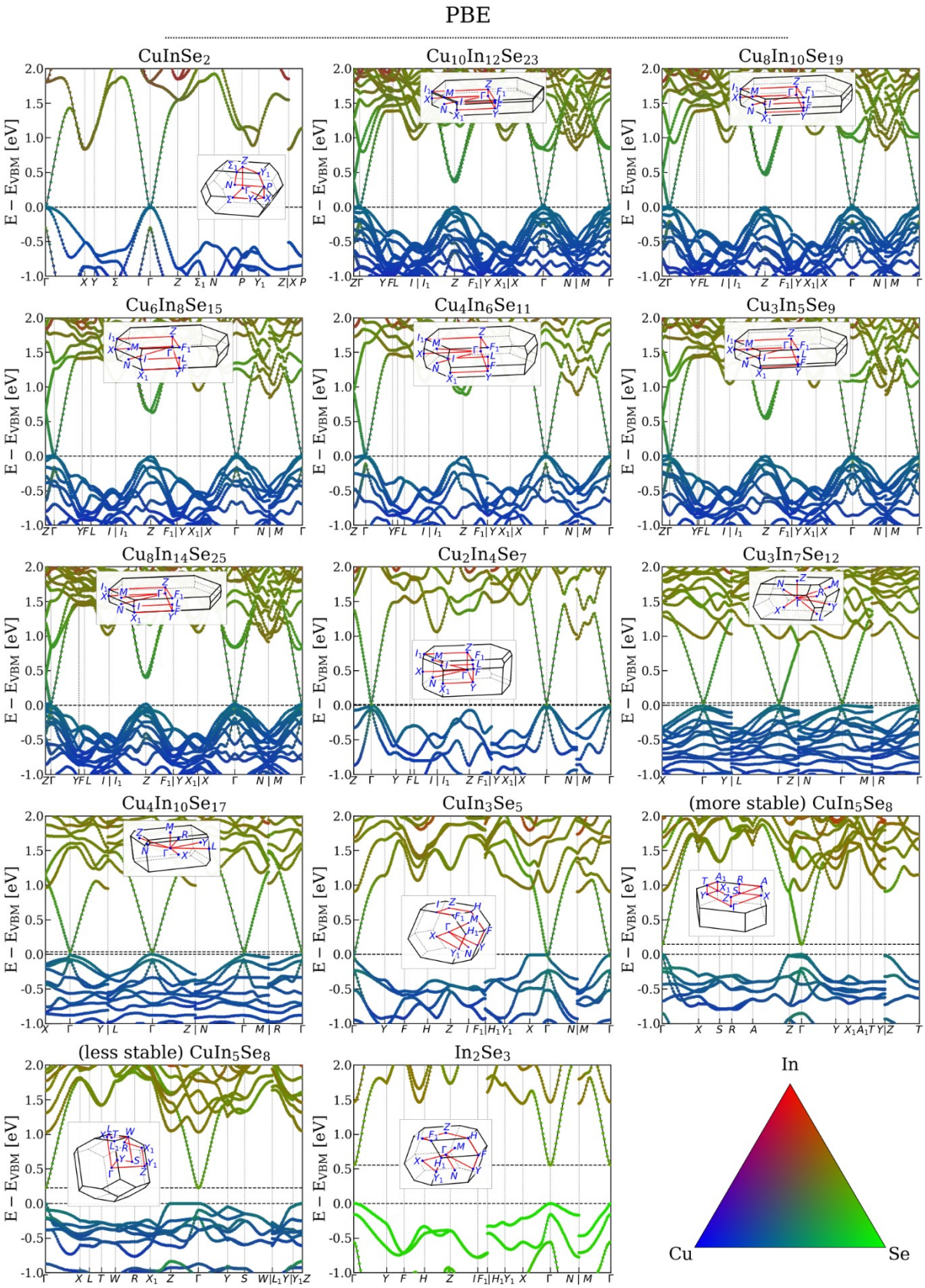

Figure S7. Element-projected band structures of (near-)stable Cu-In-Se structures computed using the PBE functional. The insets illustrate the Brillouin zones. All calculations were done for the PBEsol-optimized geometries. No adjustment of band gaps was performed.

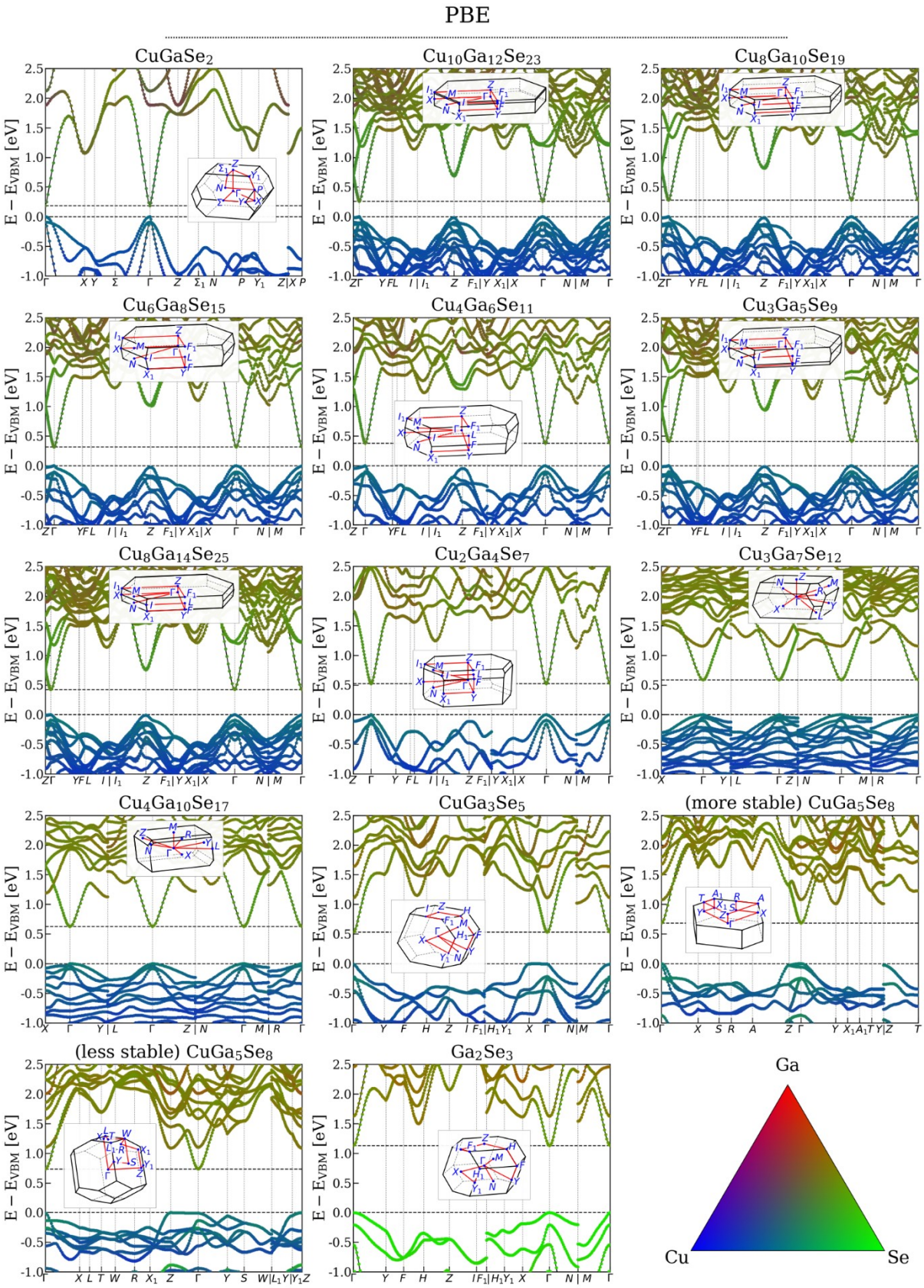

Figure S8. Element-projected band structures of (near-)stable Cu-Ga-Se structures computed using the PBE functional. The insets illustrate the Brillouin zones. All calculations were done for the PBEsol-optimized geometries. No adjustment of band gaps was performed.

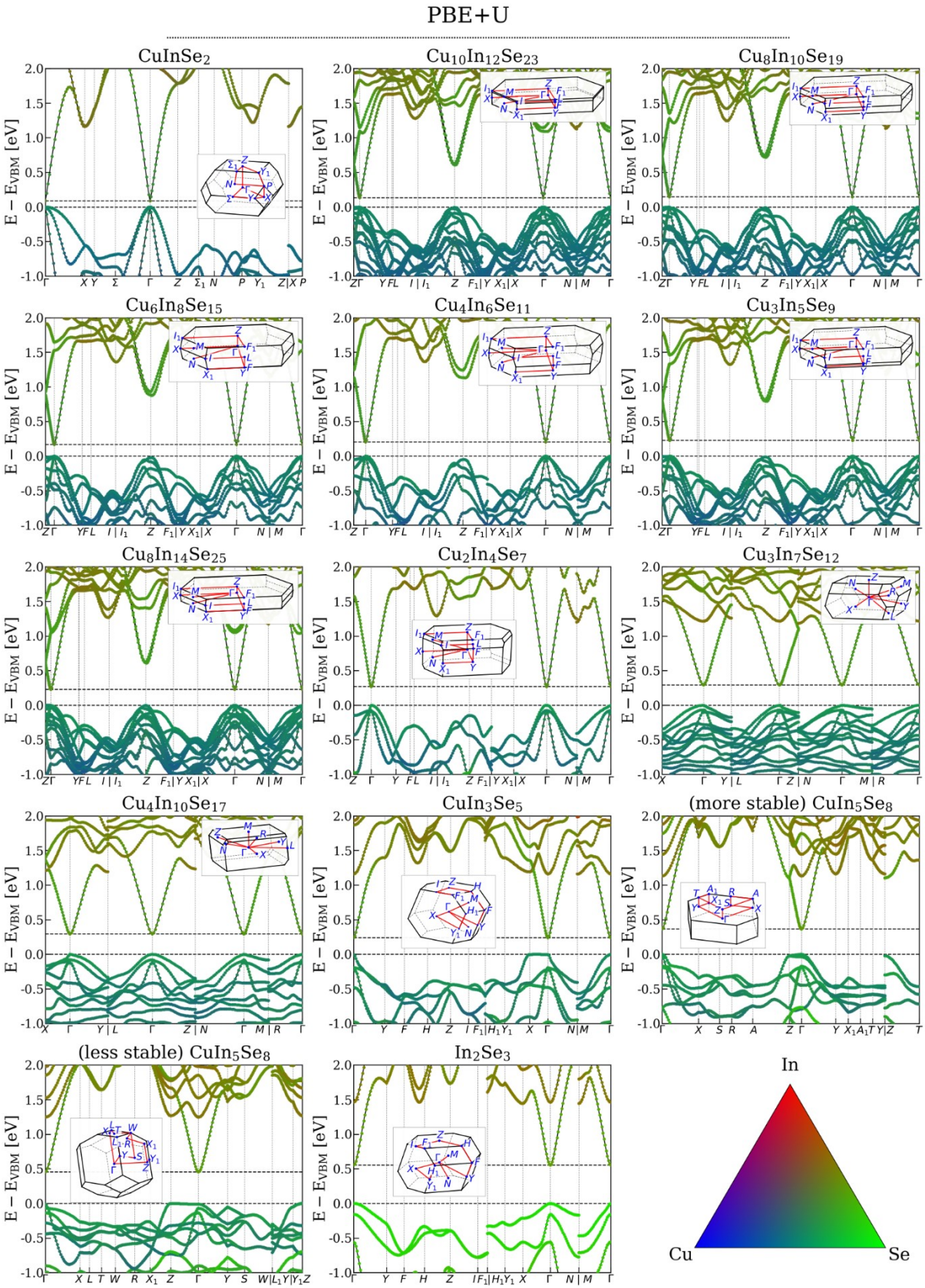

Figure S9. Element-projected band structures of (near-)stable Cu-In-Se structures computed using the PBE+U functional. The insets illustrate the Brillouin zones. All calculations were done for the PBEsol-optimized geometries. No adjustment of band gaps was performed.

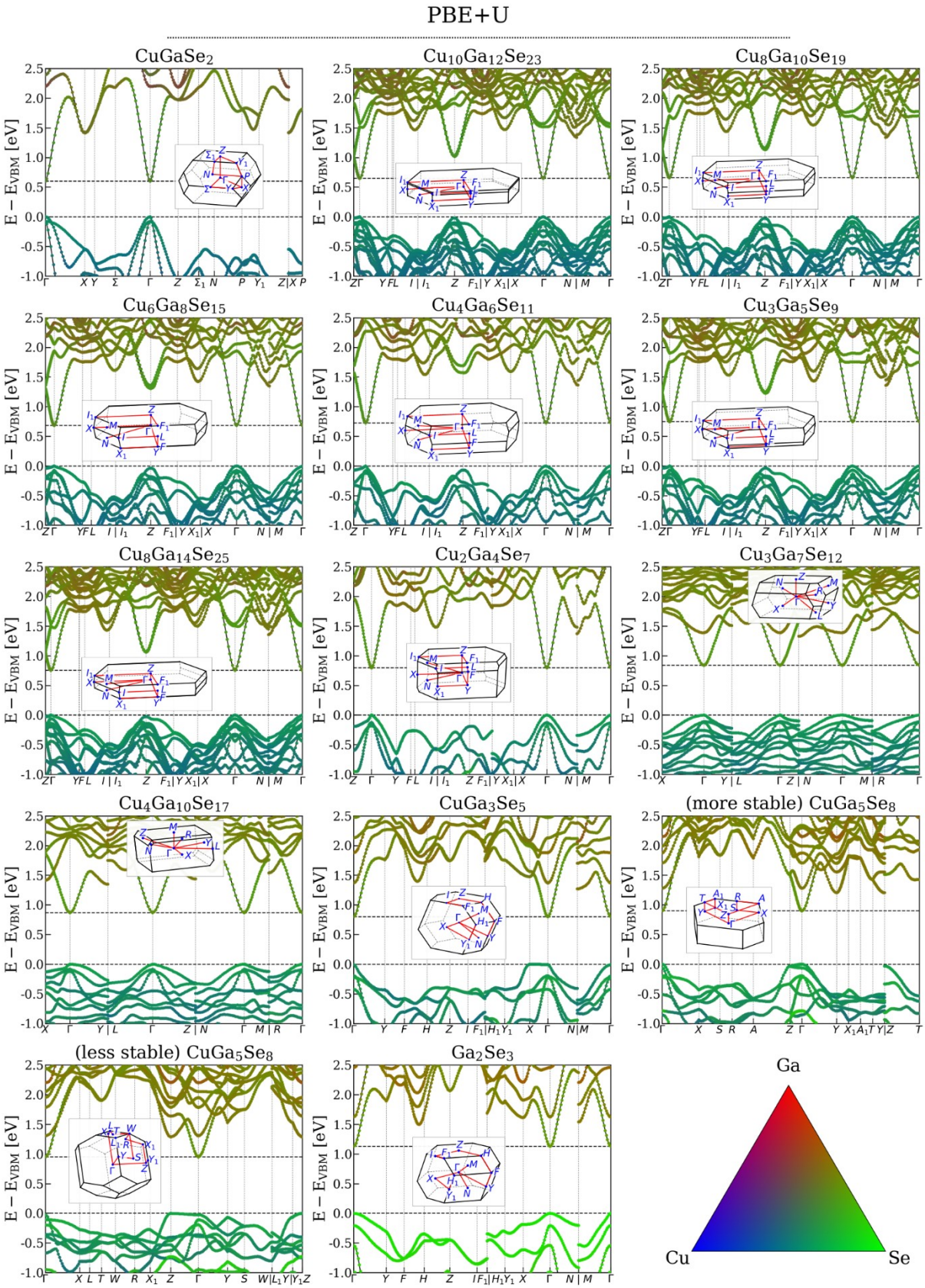

Figure S10. Element-projected band structures of (near-)stable Cu-Ga-Se structures computed using the PBE+U functional. The insets illustrate the Brillouin zones. All calculations were done for the PBEsol-optimized geometries. No adjustment of band gaps was performed.

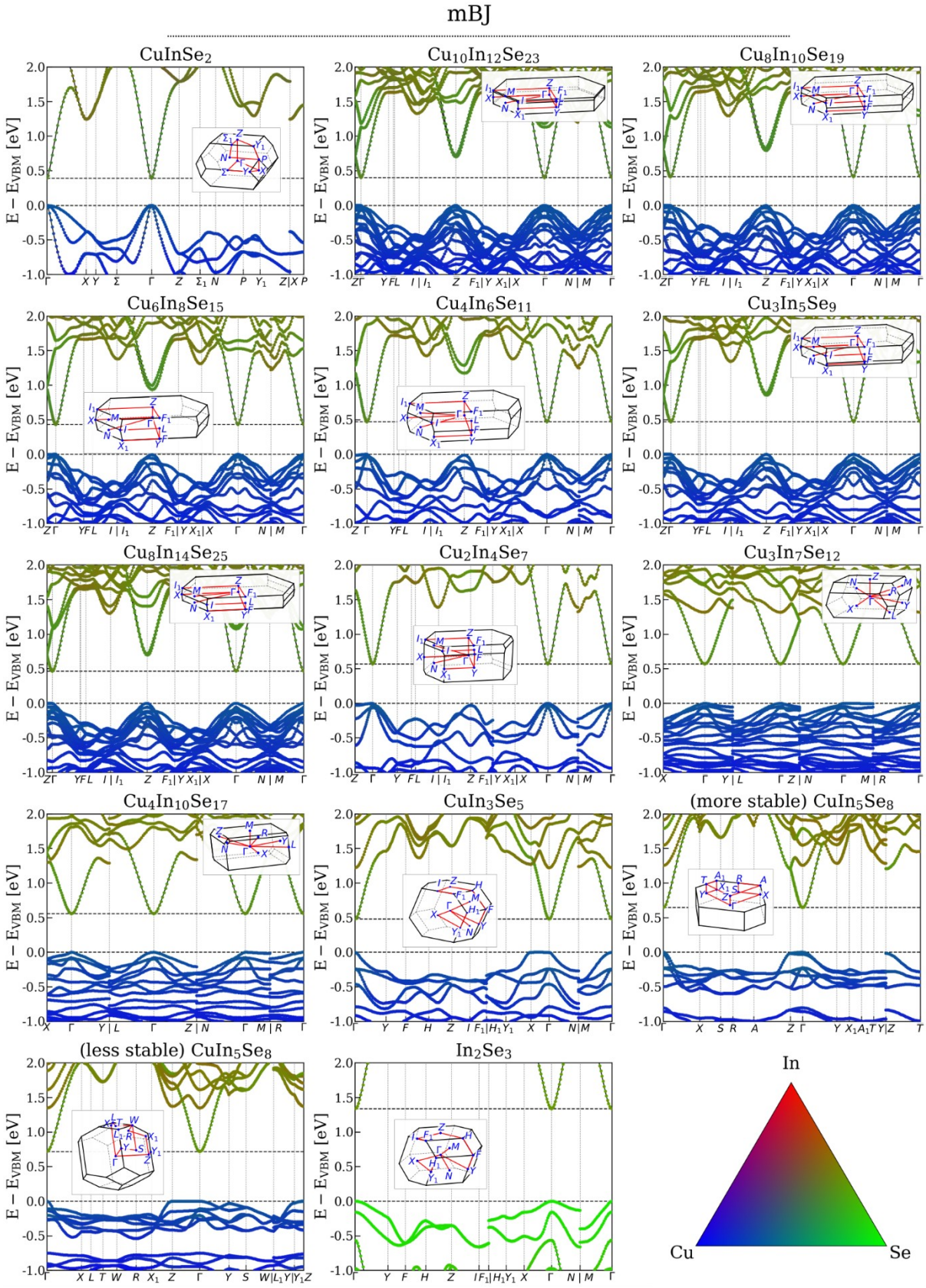

Figure S11. Element-projected band structures of (near-)stable Cu-In-Se structures computed using the mBJ functional. The insets illustrate the Brillouin zones. All calculations were done for the PBEsol-optimized geometries. No adjustment of band gaps was performed.

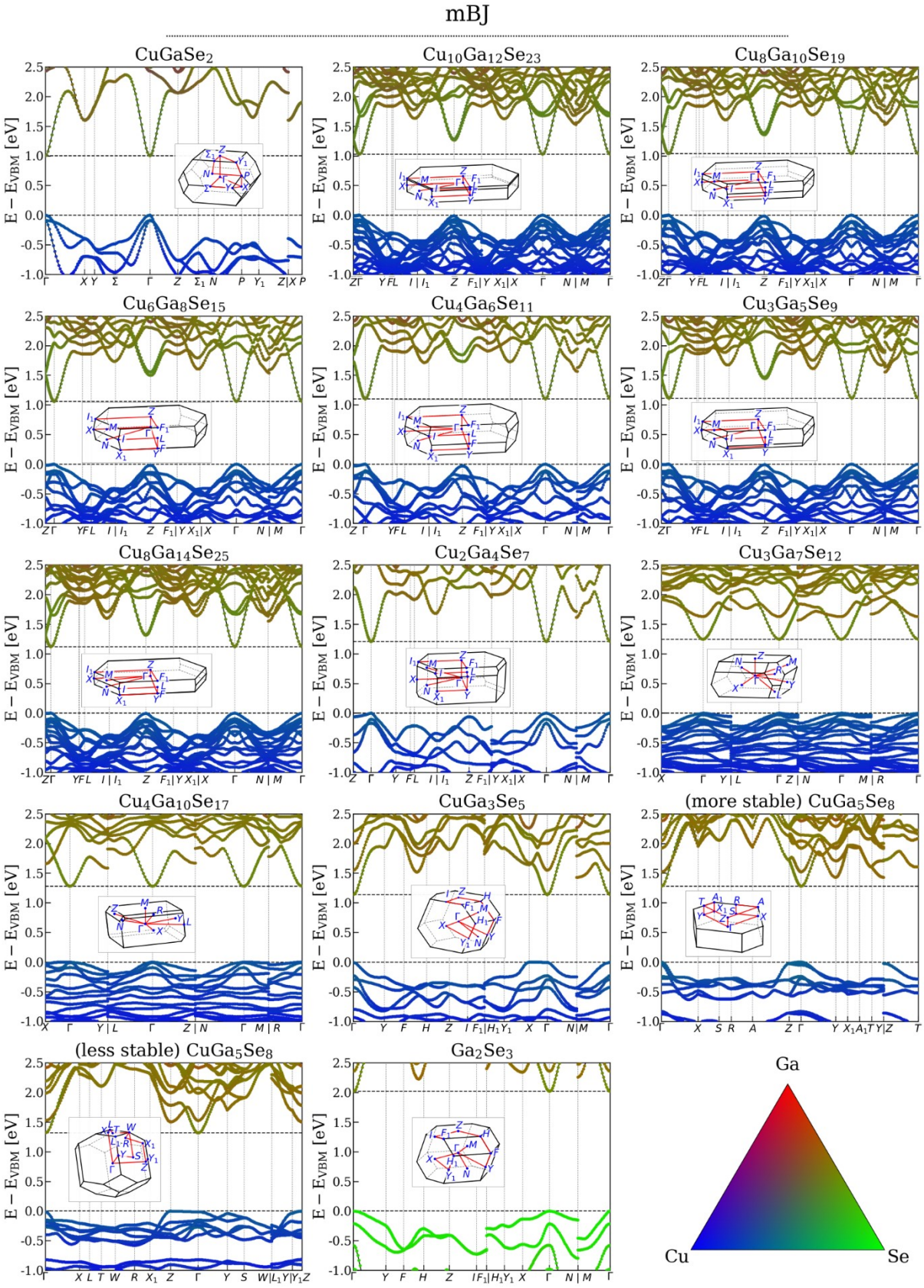

Figure S12. Element-projected band structures of (near-)stable Cu-Ga-Se structures computed using the mBJ functional. The insets illustrate the Brillouin zones. All calculations were done for the PBEsol-optimized geometries. No adjustment of band gaps was performed.

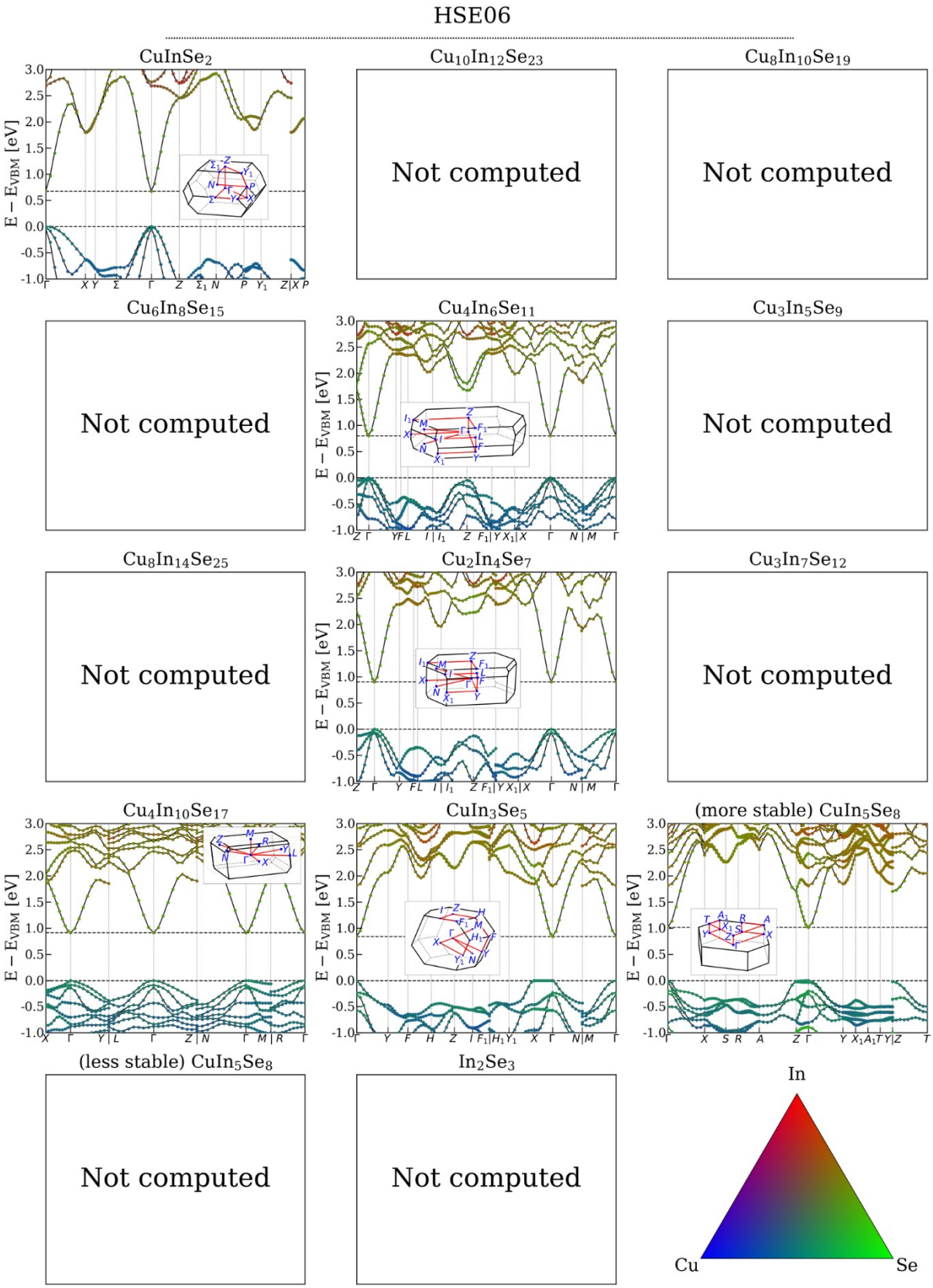

Figure S13. Element-projected band structures of (near-)stable Cu-In-Se structures computed using the HSE06 functional. The insets illustrate the Brillouin zones. All calculations were done for the PBEsol-optimized geometries. No adjustment of band gaps was performed.

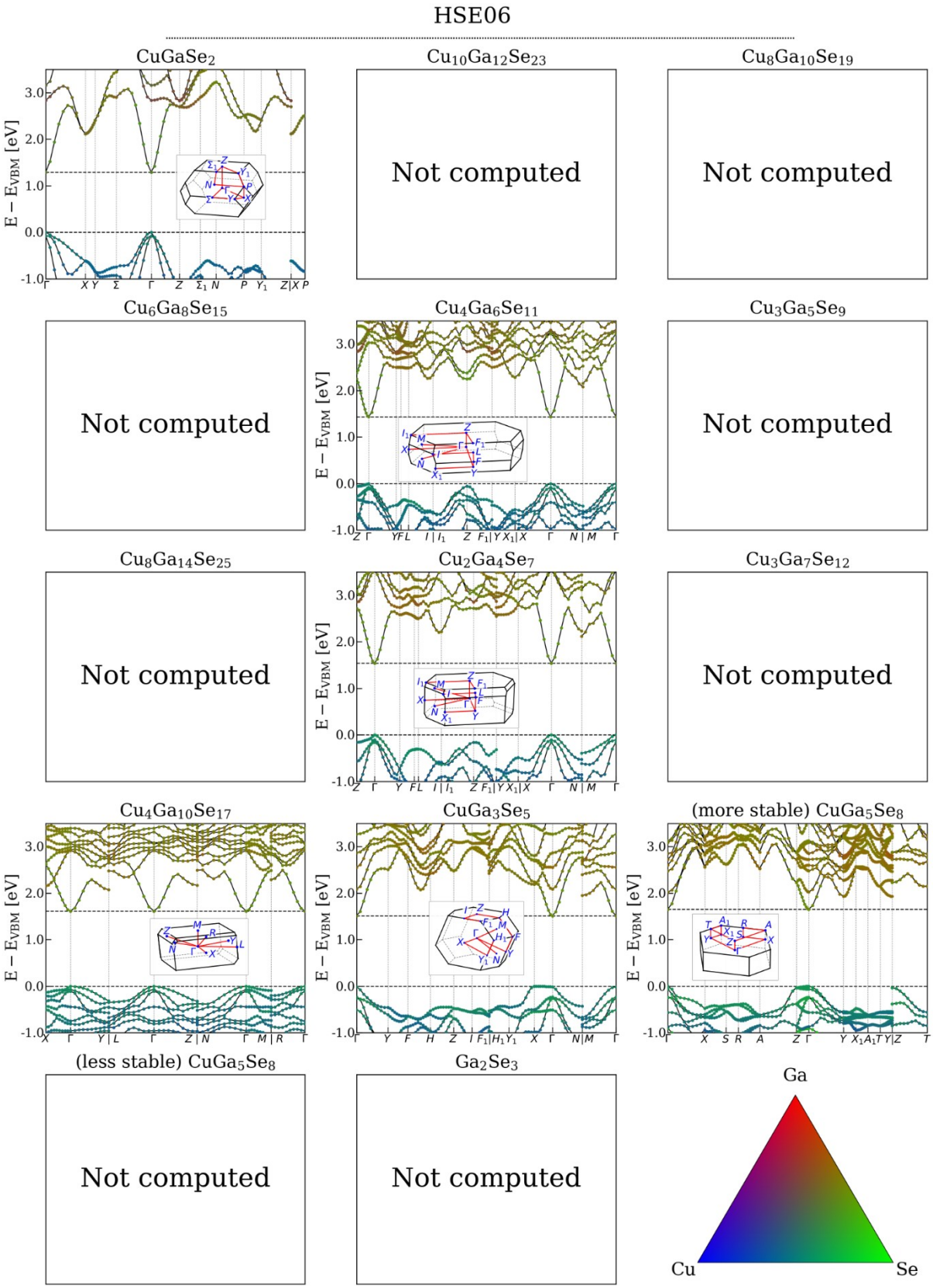

Figure S14. Element-projected band structures of (near-)stable Cu-Ga-Se structures computed using the HSE06 functional. The insets illustrate the Brillouin zones. All calculations were done for the PBEsol-optimized geometries. No adjustment of band gaps was performed.

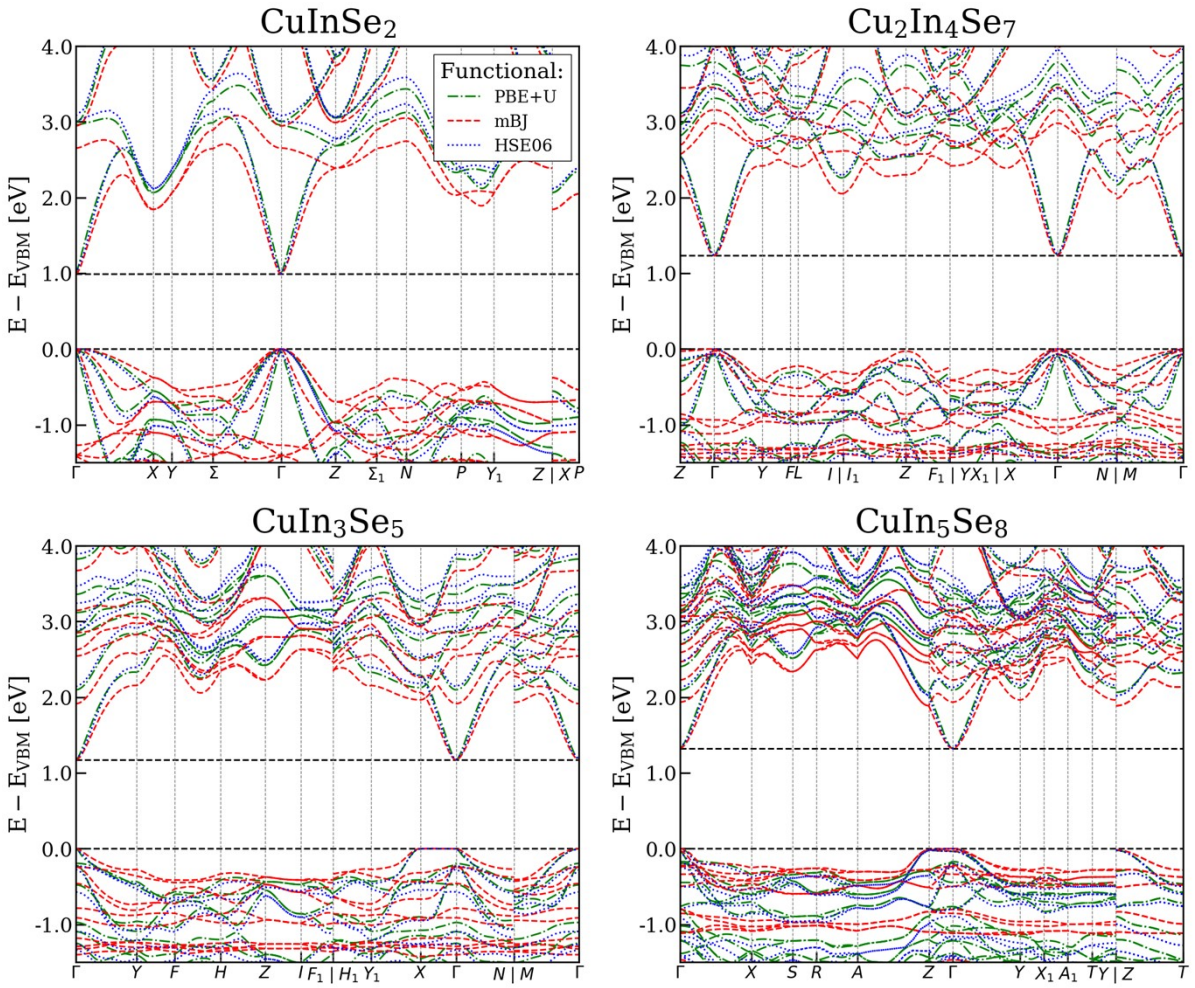

Figure S15. Comparison of band structures computed using different functionals for four selected (near-)stable Cu-In-Se structures. All calculations were performed for the PBEsol-optimized geometries. All band gaps were adjusted to the scissor-corrected HSE06 values (see Fig. 2). The PBE results are omitted due to the metallic character (zero band gap) erroneously predicted for some structures.

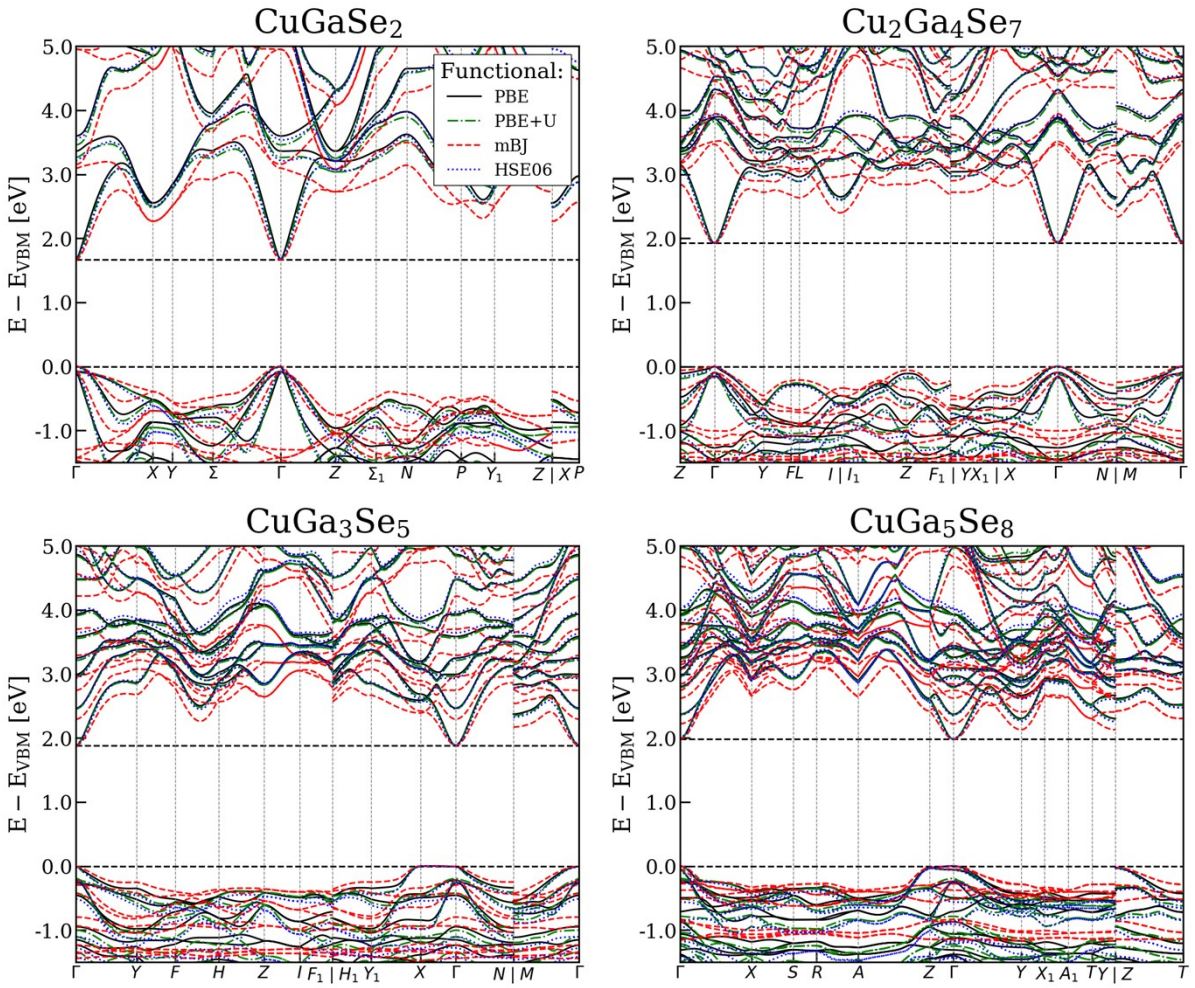

Figure S16. Comparison of band structures computed using different functionals for four selected (near-)stable Cu-Ga-Se structures. All calculations were performed for the PBEsol-optimized geometries. All band gaps were adjusted to the scissor-corrected HSE06 values (see Fig. 2).

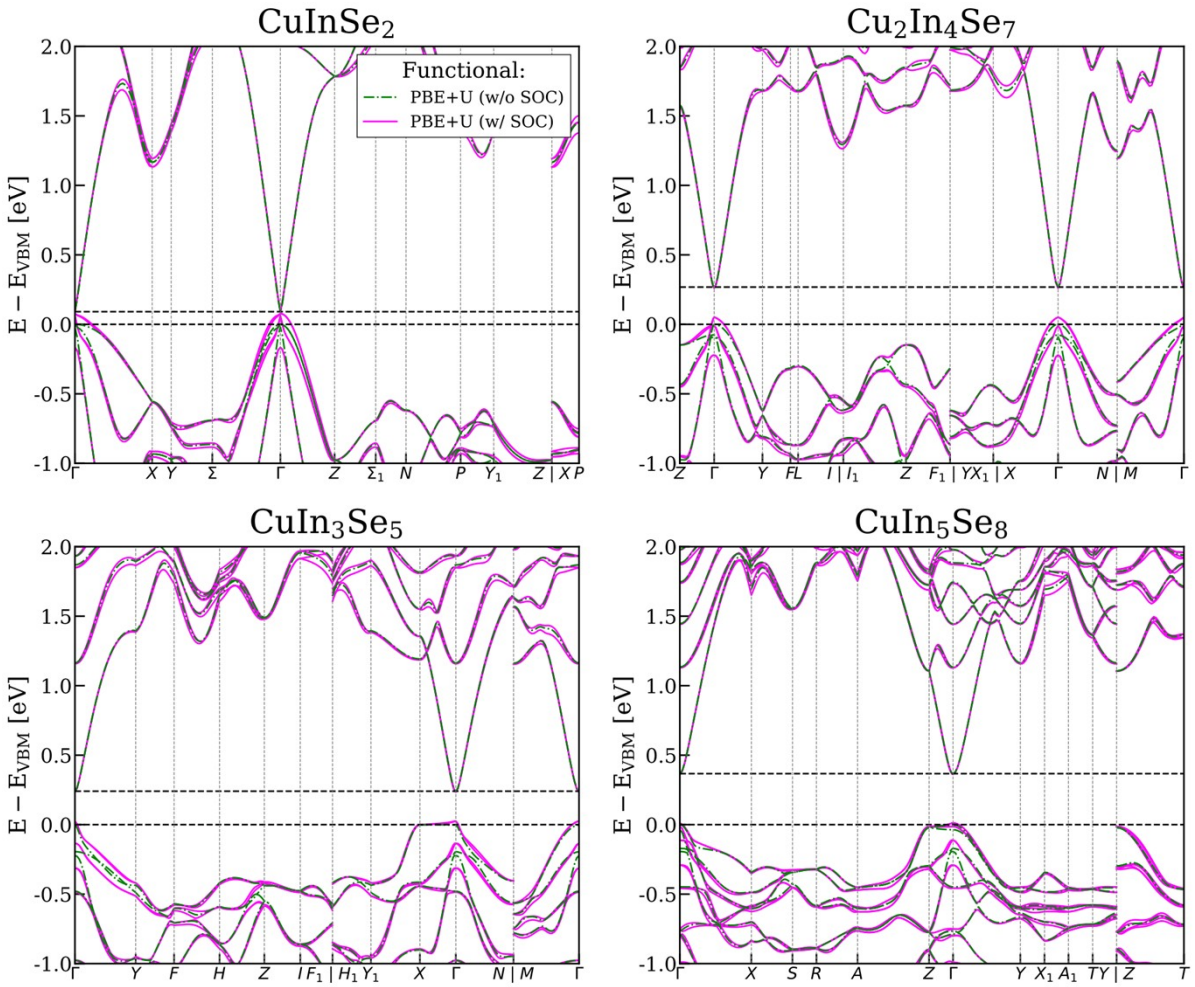

Figure S17. Comparison of band structures calculated using the PBE+U functional with and without spin-orbit coupling (SOC) for four selected (near-)stable Cu-In-Se structures. All calculations were performed for the PBEsol-optimized geometries. For the calculations with SOC, the band energies were rigidly shifted upward by up to 0.1 eV to align the dispersion curves across the Brillouin zone for ease of comparison. No band gap correction was applied.

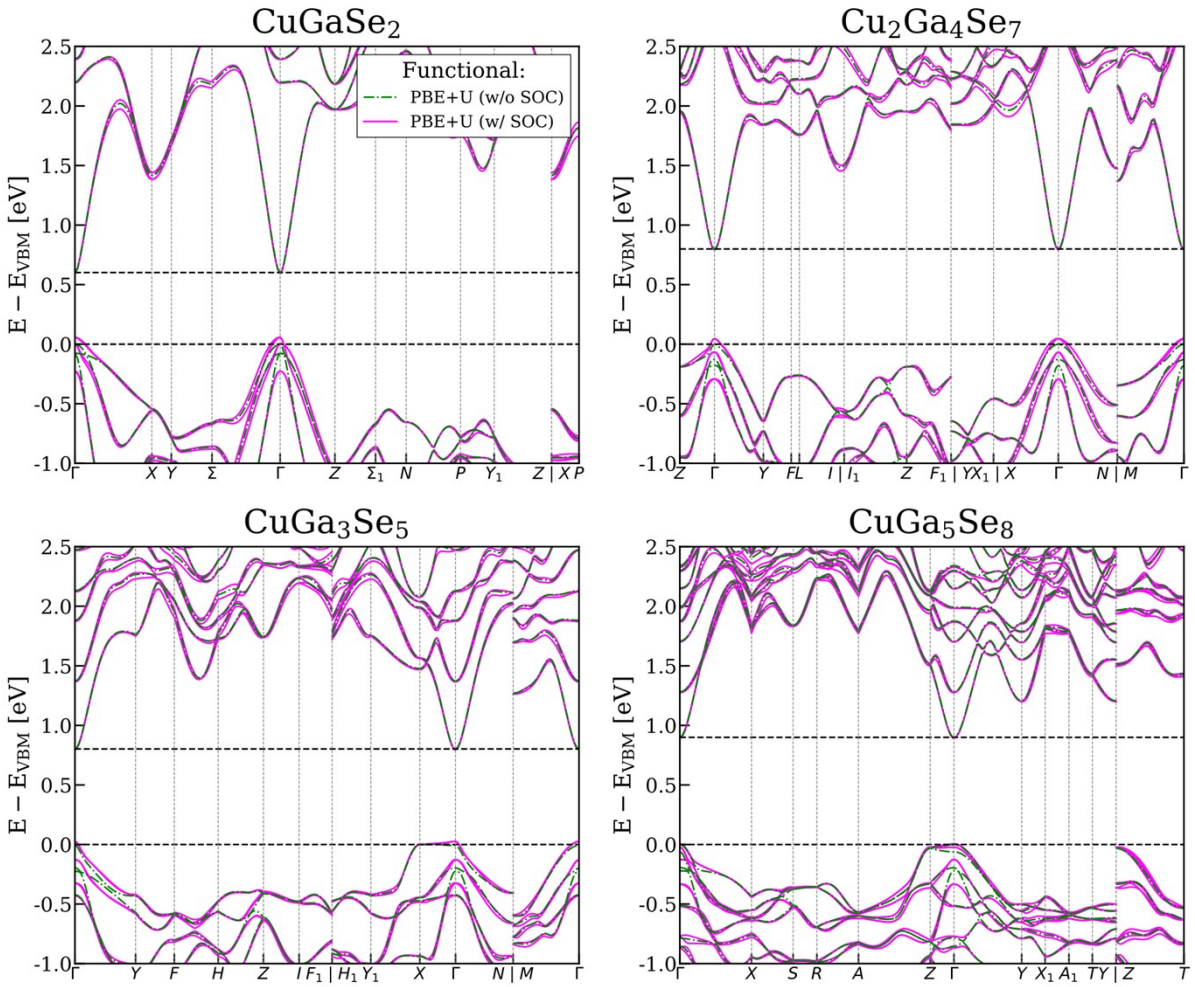

Figure S18. Comparison of band structures calculated using the PBE+U functional with and without spin-orbit coupling (SOC) for four selected (near-)stable Cu-Ga-Se structures. All calculations were performed for the PBEsol-optimized geometries. For the calculations with SOC, the band energies were rigidly shifted upward by up to 0.1 eV to align the dispersion curves across the Brillouin zone for ease of comparison. No band gap correction was applied.

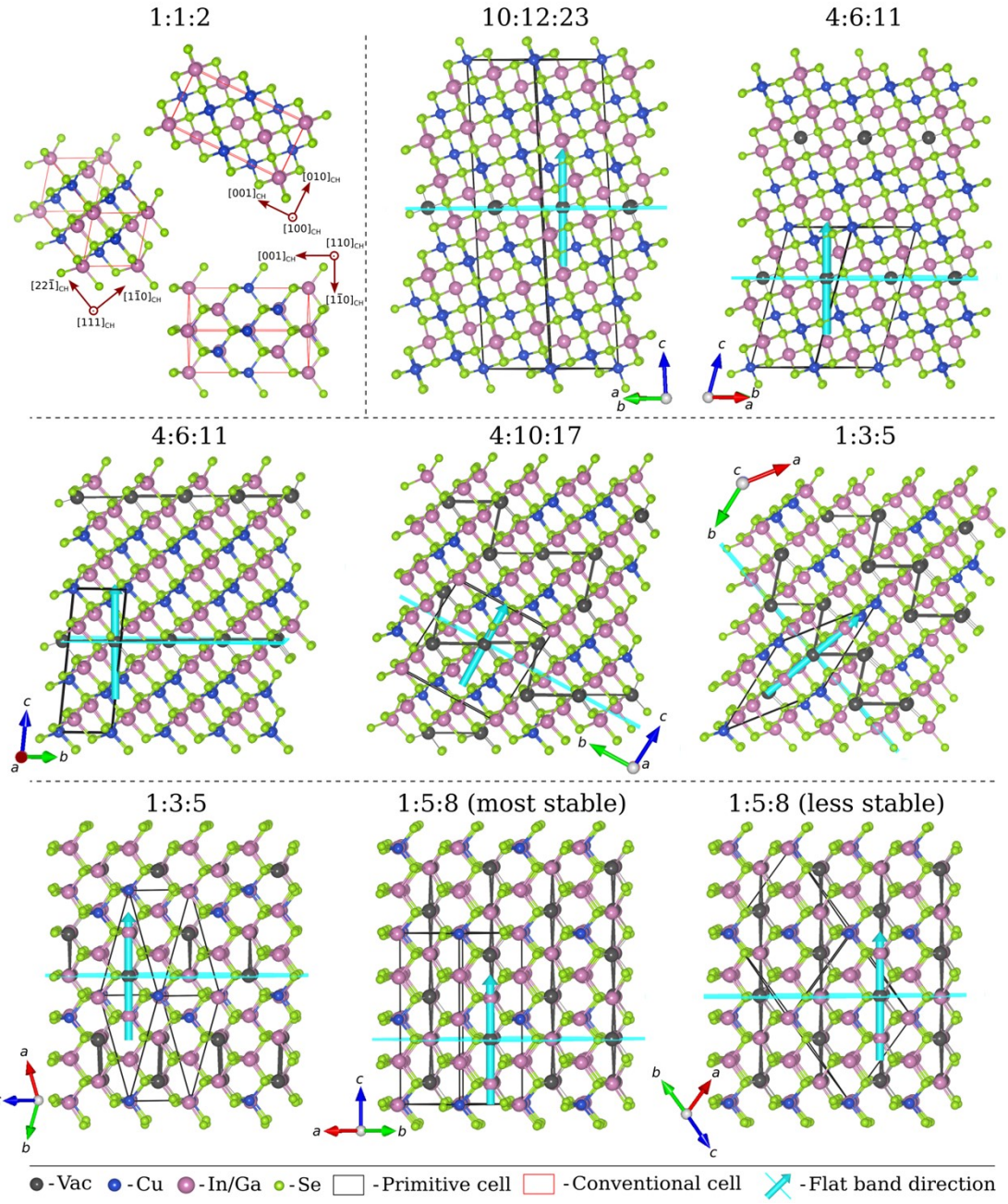

Figure S19. Illustration of the real-space directions for selected ODCs corresponding to k-space segments with a flat valence band edge in the band structure (i.e., X-Γ for the 1:3:5 structure, M-Γ for the 4:10:17 structure, and Z-Γ for all other ODCs). Different projections of the conventional chalcopyrite unit cell are shown for comparison.

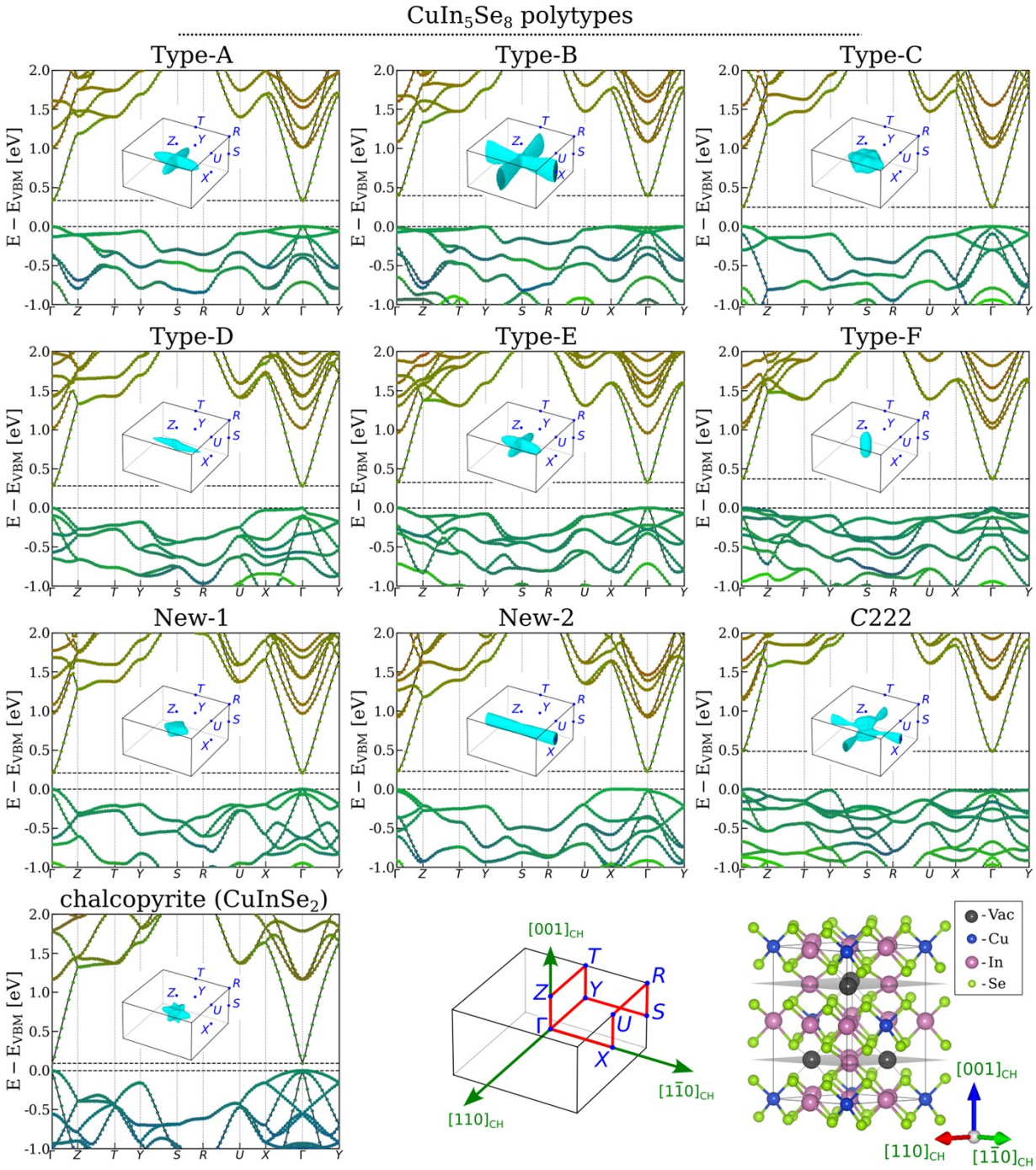

Figure S20. Element-projected band structures of the nine literature $CuIn_5Se_8$ polytypes (see Table S1) and chalcopyrite $CuInSe_2$, calculated using the PBE+U functional. All calculations were performed using the PBEsol-optimized geometries. The calculations employed the same unit cell geometry (aside from minor structural relaxations) and, consequently, the same Brillouin zone geometry, as illustrated for the "Type-D" polytype in the bottom row. The insets show the Fermi surfaces calculated at the valence band edge (i.e., 26 meV below VBM). No band gap correction was applied.

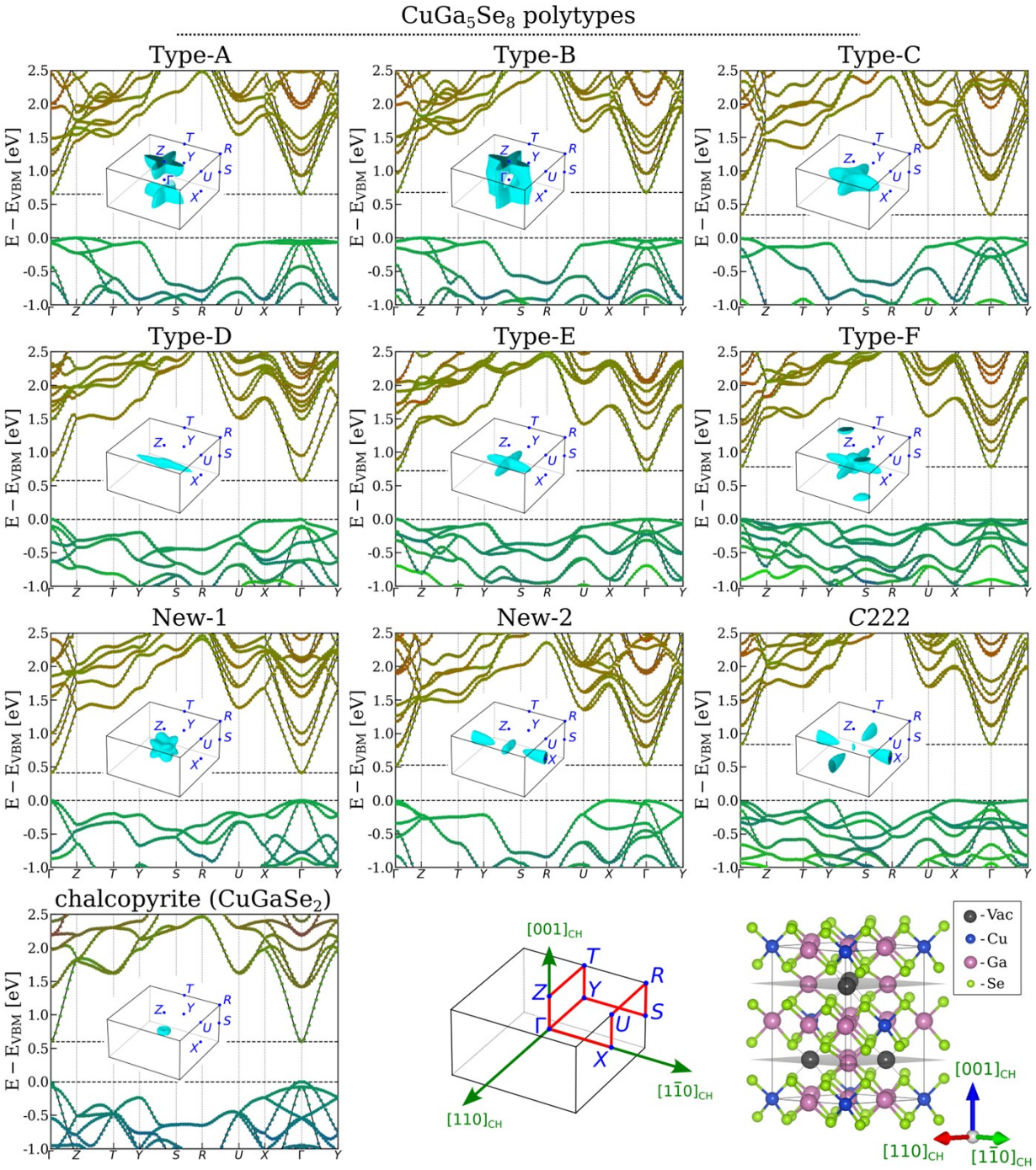

Figure S21. Element-projected band structures of the nine literature $CuGa_5Se_8$ polytypes (see Table S1) and chalcopyrite $CuGaSe_2$, calculated using the PBE+U functional. All calculations were performed using the PBEsol-optimized geometries. The calculations employed the same unit cell geometry (aside from minor structural relaxations) and, consequently, the same Brillouin zone geometry, as illustrated for the "Type-D" polytype in the bottom row. The insets show the Fermi surfaces calculated at the valence band edge (i.e., 26 meV below VBM). No band gap correction was applied.

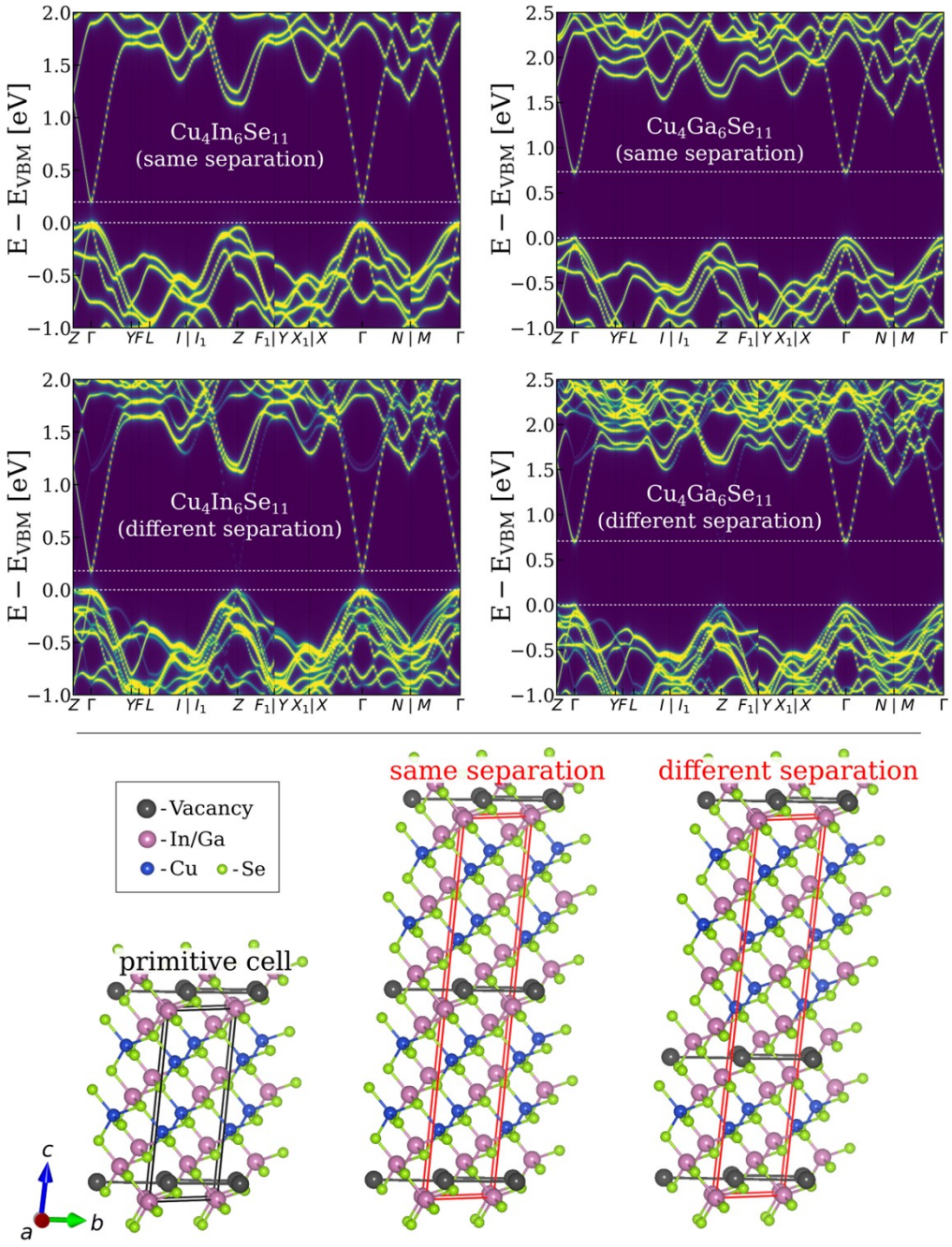

Figure S22. Band structures of two $Cu_4In_6Se_{11}$ and $Cu_4Ga_6Se_{11}$ polytypes ("same separation" and "different separation," defined by the distribution of Cu-poor planar defects), computed with the PBE+U functional and unfolded into the same "primitive cell". The "same separation" structure geometry was fully optimized with the PBEsol, while the "different separation" lattice parameters were fixed to match. No band-gap correction was applied.

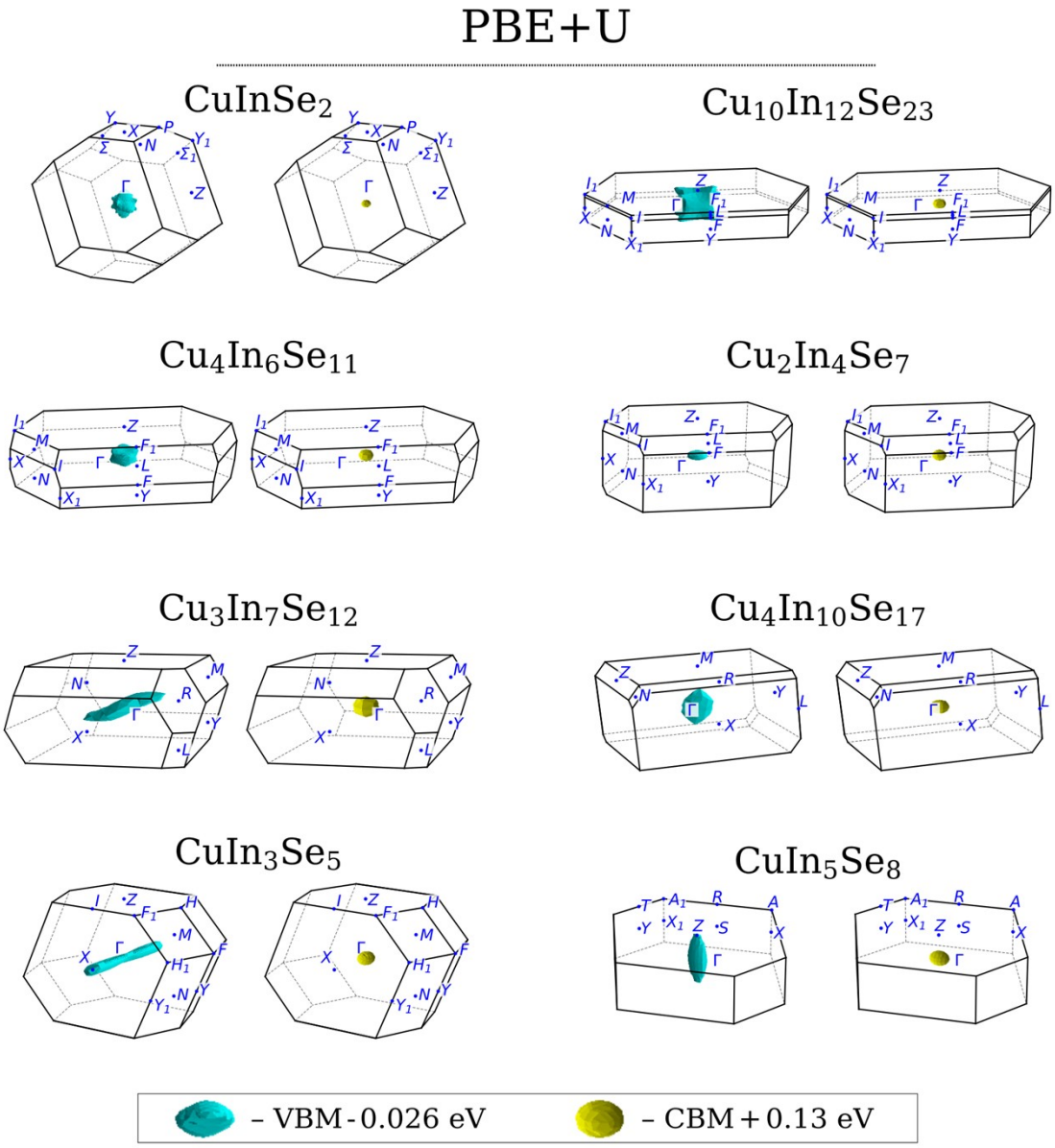

Figure S23. Fermi surfaces in the Brillouin zones of the (near-)stable structures in the Cu-In-Se system obtained with the PBE+U functional for energies 26 meV below VBM and 130 meV above CBM. All calculations were done for the PBEsol-optimized geometries. The Brillouin zones are shown with differing scales across the structures.

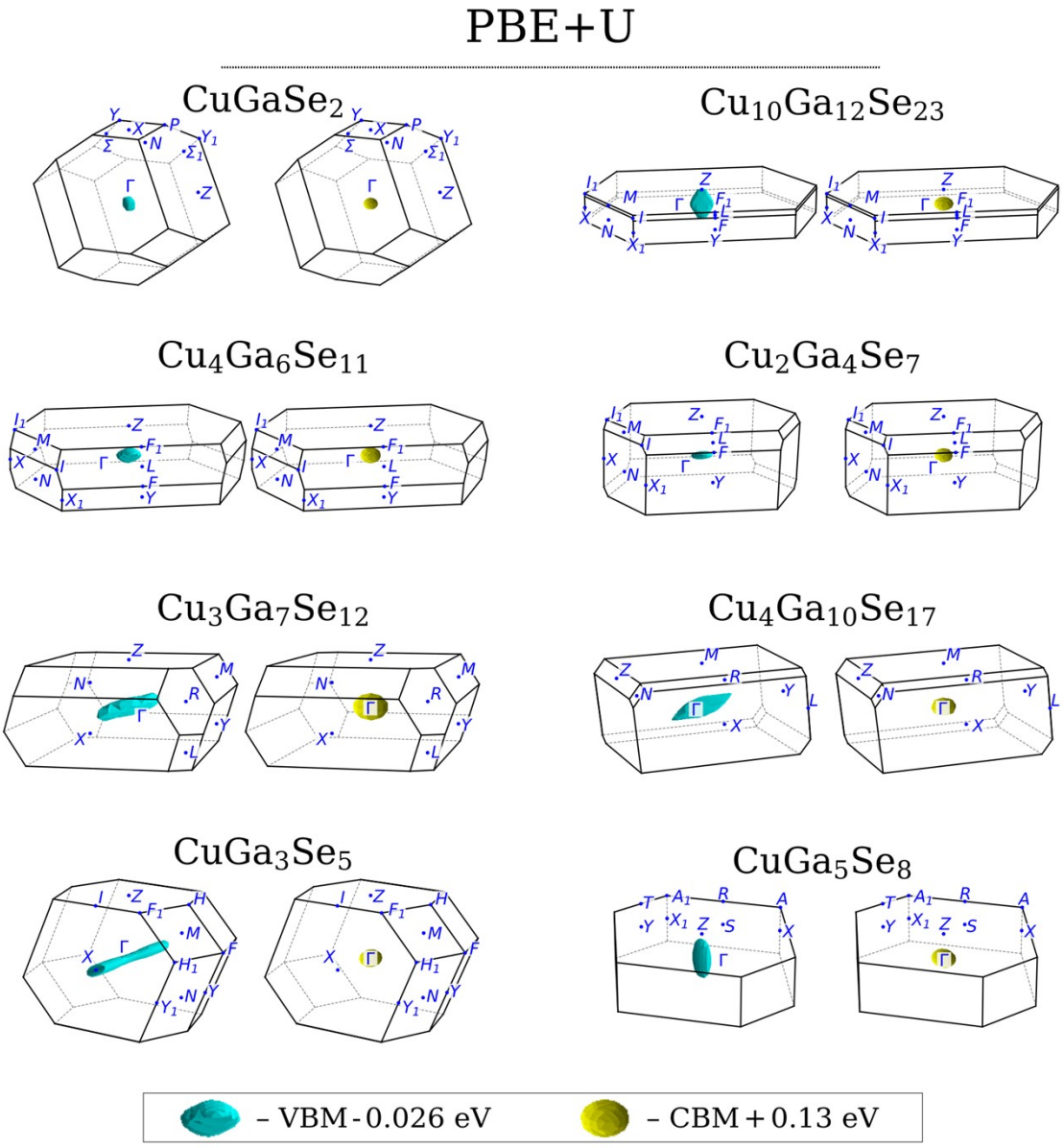

Figure S24. Fermi surfaces in the Brillouin zones of the (near-)stable structures in the Cu-Ga-Se system obtained with the PBE+U functional for energies 26 meV below VBM and 130 meV above CBM. All calculations were done for the PBEsol-optimized geometries. The Brillouin zones are shown with differing scales across the structures.

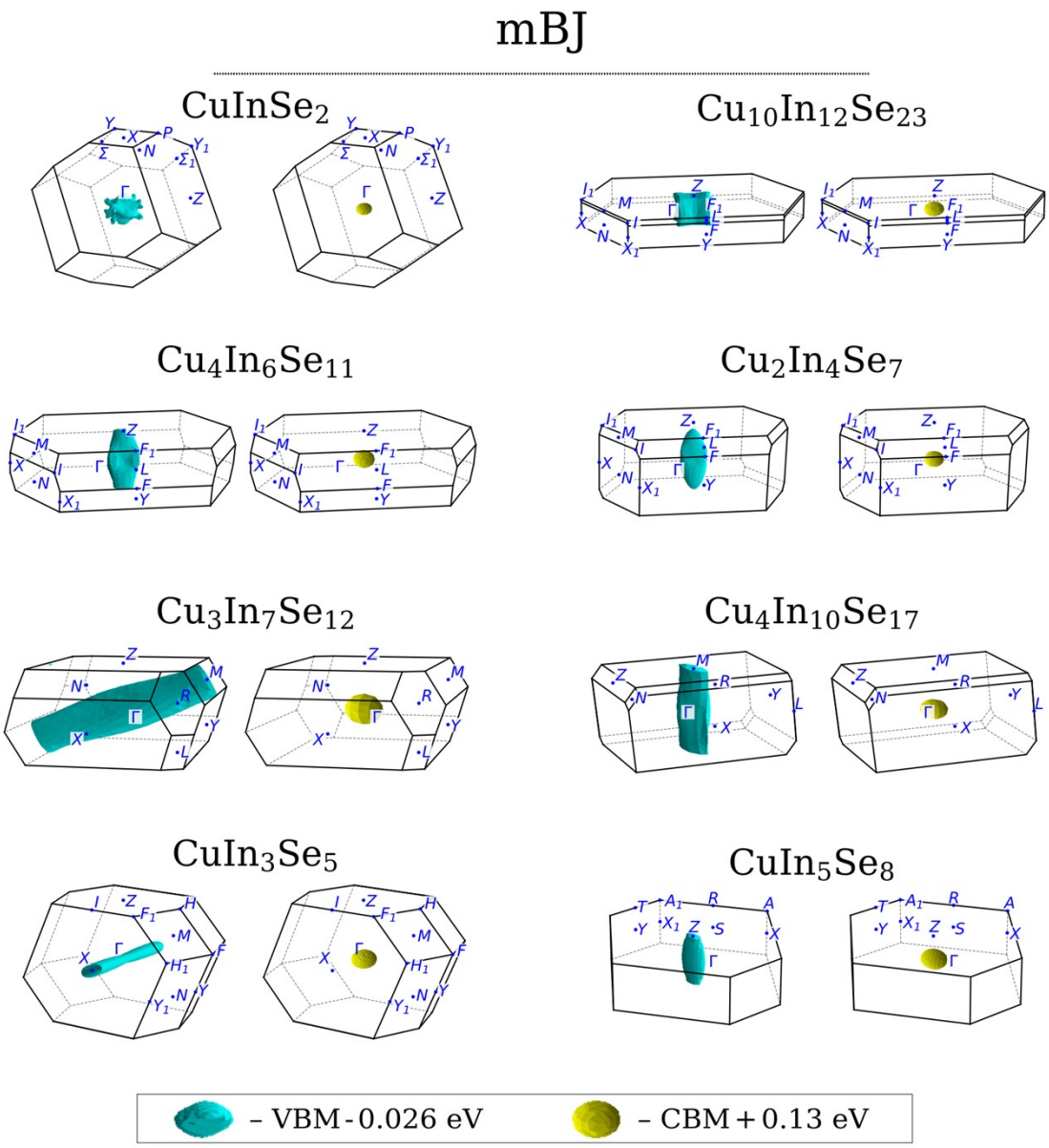

Figure S25. Fermi surfaces in the Brillouin zones of the (near-)stable structures in the Cu-In-Se system obtained with the mBJ functional for energies 26 meV below VBM and 130 meV above CBM. All calculations were done for the PBEsol-optimized geometries. The Brillouin zones are shown with differing scales across the structures.

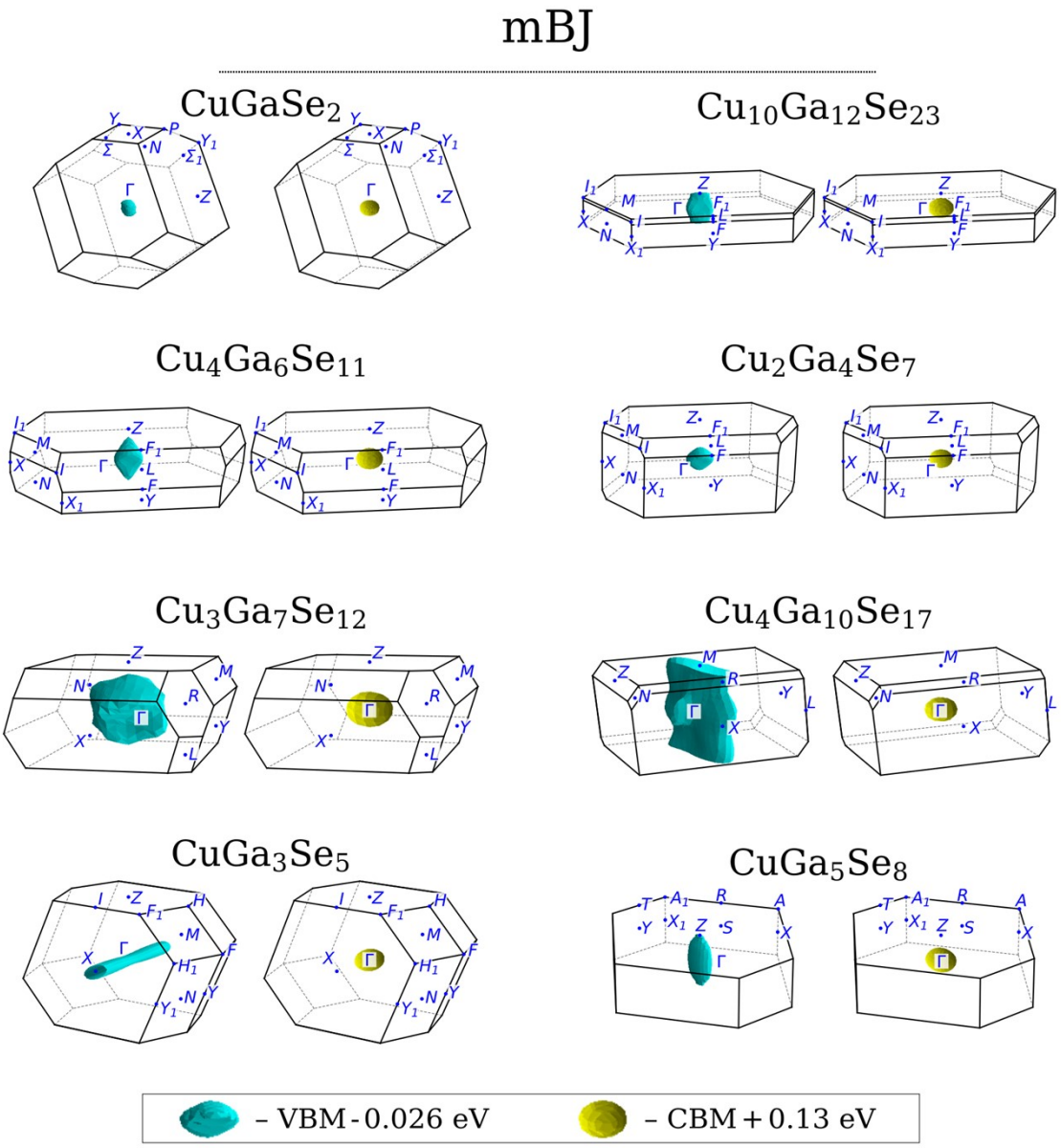

Figure S26. Fermi surfaces in the Brillouin zones of the (near-)stable structures in the Cu-Ga-Se system obtained with the mBJ functional for energies 26 meV below VBM and 130 meV above CBM. All calculations were done for the PBEsol-optimized geometries. The Brillouin zones are shown with differing scales across the structures.

References

1 C. D. R. Ludwig, T. Gruhn, C. Felser and J. Windeln, *Phys. Rev. B*, 2011, **83**, 174112.
2 C.-H. Chang, S.-H. Wei, J. W. Johnson, S. B. Zhang, N. Leyarovska, G. Bunker and T. J. Anderson, *Phys. Rev. B*, 2003, **68**, 054108.
3 A. Jain, S. P. Ong, G. Hautier, W. Chen, W. D. Richards, S. Dacek, S. Cholia, D. Gunter, D. Skinner, G. Ceder and K. A. Persson, *APL Mater.*, 2013, **1**, 011002.
4 W. Liu, H. Liang, Y. Duan and Z. Wu, *Phys. Rev. Materials*, 2019, **3**, 125405.
5 X. Chen, W. Liu and Y. Duan, *J. Phys.: Condens. Matter*, 2020, **33**, 075401.
6 S. Kirklin, J. E. Saal, B. Meredig, A. Thompson, J. W. Doak, M. Aykol, S. Rühl and C. Wolverton, *npj Comput. Mater.*, 2015, **1**, 1–15.
7 S. B. Zhang, S.-H. Wei and A. Zunger, *Phys. Rev. Lett.*, 1997, **78**, 4059–4062.
8 S. B. Zhang, S.-H. Wei, A. Zunger and H. Katayama-Yoshida, *Phys. Rev. B*, 1998, **57**, 9642–9656.
9 E. Ghorbani, J. Kiss, H. Mirhosseini, G. Roma, M. Schmidt, J. Windeln, T. D. Kühne and C. Felser, *J. Phys. Chem. C*, 2015, **119**, 25197–25203.
10 J. Kiss, T. Gruhn, G. Roma and C. Felser, *J. Phys. Chem. C*, 2013, **117**, 10892–10900.
11 J. Kiss, T. Gruhn, G. Roma and C. Felser, *J. Phys. Chem. C*, 2013, **117**, 25933–25938.
12 H. Xiao and W. A. Goddard, *J. Chem. Phys.*, 2014, **141**, 094701.
13 J. Pohl and K. Albe, *Phys. Rev. B*, 2013, **87**, 245203.
14 M. Malitckaya, T. Kunze, H.-P. Komsa, V. Havu, E. Handick, R. G. Wilks, M. Bär and M. J. Puska, *ACS Appl. Mater. Interfaces*, 2019, **11**, 3024–3033.
15 A. Sharan, F. P. Sabino, A. Janotti, N. Gaillard, T. Ogitsu and J. B. Varley, *J. Appl. Phys.*, 2020, **127**, 065303.
16 T. Maeda, W. Gong and T. Wada, *Jpn. J. Appl. Phys.*, 2016, **55**, 04ES15.
17 F. Jiang and J. Feng, *Appl. Phys. Lett.*, 2006, **89**, 221920.
18 S. Kumar, S. Joshi and S. Auluck, *Mater. Chem. Phys.*, 2015, **162**, 372–379.
19 L.-H. Tu, N. T. T. Tran, S.-K. Lin and C.-H. Lai, *Adv. Energy Mater.*, 2023, **13**, 2301227.
20 S. Lehmann, D. F. Marrón, M. León, R. Feyerherm, E. Dudzik, E. J. Friedrich, M. Tovar, Y. Tomm, C. Wolf, S. Schorr, Th. Schedel-Niedrig, M. Ch. Lux-Steiner and J. M. Merino, *J. Appl. Phys.*, 2011, **109**, 013518.
21 M. Yarema, N. Yazdani, O. Yarema, N. Đorđević, W. M. M. Lin, D. Bozyigit, S. Volk, A. Moser, A. Turrini, P. A. Khomyakov, M. Nachtegaal, M. Luisier and V. Wood, *Adv. Mater.*, 2024, **36**, 2406351.
22 A. Moser, O. Yarema, N. Rusch, N. Đorđević, W. M. M. Lin, D. Bozyigit, N. Yazdani, M. Yarema, M. Luisier and V. Wood, *ACS Nanosci. Au*, 2024, **5**, 21–28.
23 G. Marín, S. M. Wasim, C. Rincón, G. Sánchez Pérez, Ch. Power and A. E. Mora, *J. Appl. Phys.*, 1998, **83**, 3364–3366.
24 C. Rincón, S. M. Wasim, G. Marín and I. Molina, *J. Appl. Phys.*, 2002, **93**, 780–782.
25 G. Marín, S. Tauleigne, S. M. Wasim, R. Guevara, J. M. Delgado, C. Rincón, A. E. Mora and G. Perez, *Mater. Res. Bull.*, 1998, **33**, 1057–1068.
26 C.-D. Kim, M.-S. Jin and W.-T. Kim, *J. Korean Phys. Soc.*, 1998, **32**, 750.
27 T. Negami, N. Kohara, M. Nishitani, T. Wada and T. Hirao, *Appl. Phys. Lett.*, 1995, **67**, 825–827.
28 M. León, R. Serna, S. Levcenko, A. Nateprov, A. Nicorici, J. M. Merino and E. Arushanov, *J. Appl. Phys.*, 2007, **101**, 013524.
29 M. León, R. Serna, S. Levcenko, A. Nateprov, A. Nicorici, J. M. Merino and E. Arushanov, *Phys. Status Solidi A*, 2006, **203**, 2913–2918.
30 M. A. Contreras, L. M. Mansfield, B. Egaas, J. Li, M. Romero, R. Noufi, E. Rudiger-Voigt and W. Mannstadt, *Prog. Photovolt.: Res. Appl.*, 2012, **20**, 843–850.
31 M. I. Alonso, K. Wakita, J. Pascual, M. Garriga and N. Yamamoto, *Phys. Rev. B*, 2001, **63**, 075203.
32 S. Levcenko, N. N. Syrbu, E. Arushanov, V. Tezlevan, R. Fernández-Ruiz, J. M. Merino and M. León, *J. Appl. Phys.*, 2006, **99**, 073513.

33 E. J. Friedrich, J. F. Trigo, J. Ramiro, C. Guillén, J. M. Merino and M. León, *J. Phys. D: Appl. Phys.*, 2009, **42**, 085401.
34 Y. B. K. Reddy and V. S. Raja, *Mater. Lett.*, 2004, **58**, 1839–1843.
35 D. Schmid, M. Ruckh, F. Grunwald and H. W. Schock, *J. Appl. Phys.*, 1993, **73**, 2902–2909.
36 L. Durán, C. Guerrero, E. Hernández, J. M. Delgado, J. Contreras, S. M. Wasim and C. A. Durante Rincón, *J. Phys. Chem. Solids*, 2003, **64**, 1907–1910.
37 R. R. Philip and B. Pradeep, *Semicond. Sci. Technol.*, 2003, **18**, 768.
38 Ariswan, G. El haj Moussa, M. Abdelali, F. Guastavino and C. Llinares, *Solid State Commun.*, 2002, **124**, 391–396.
39 E. Hernández, L. Durán, C. A. Durante Rincón, G. Aranguren, C. Guerrero and J. Naranjo, *Cryst. Res. Technol.*, 2002, **37**, 1227–1233.
40 G. Marín, C. Rincón, S. M. Wasim, G. Sánchez Pérez and I. Molina, *J. Alloys Compd.*, 1999, **283**, 1–4.
41 J. L. Shay and B. Tell, *Surf. Sci.*, 1973, **37**, 748–762.
42 K. Ueda, T. Maeda and T. Wada, *Thin Solid Films*, 2017, **633**, 23–30.
43 S. Levcenko, N. N. Syrbu, A. Nateprov, E. Arushanov, J. M. Merino and M. León, *J. Phys. D: Appl. Phys.*, 2006, **39**, 1515.
44 S. M. Wasim, C. Rincón, G. Marín and J. M. Delgado, *Appl. Phys. Lett.*, 2000, **77**, 94–96.